PCT

WORLD INTELLECTUAL PROPERTY ORGANIZATION
International Bureau

INTERNATIONAL APPLICATION PUBLISHED UNDER THE PATENT COOPERATION TREATY (PCT)

<table>
<tr>
<td colspan="2">(51) International Patent Classification ⁷:
G01T 1/164</td>
<td>A1</td>
<td>(11) International Publication Number: WO 00/10034

(43) International Publication Date: 24 February 2000 (24.02.00)</td>
</tr>
</table>

(21) International Application Number: PCT/CA99/00751

(22) International Filing Date: 13 August 1999 (13.08.99)

(30) Priority Data:
60/096,649   14 August 1998 (14.08.98)   US

(71)(72) Applicants and Inventors: PRATO, Frank, S. [CA/CA]; 408 Briarhill Avenue, London, Ontario N5Y 1P2 (CA). STODILKA, Robert, Z. [CA/CA]; 424 The Kingsway, Etobicoke, Ontario M9A 3W1 (CA). KEMP, Brad, J. [CA/CA]; 49 Queen Mary Crescent, London, Ontario N6H 4B5 (CA). NICHOLSON, Richard, L. [CA/CA]; 7 Sir Robert Place, Arva, Ontario N0M 1C0 (CA).

(74) Agents: RUSTON, David, A. et al.; Sim & McBurney, 6th Floor, 330 University Avenue, Toronto, Ontario M5G 1R7 (CA).

(81) Designated States: AE, AL, AM, AT, AU, AZ, BA, BB, BG, BR, BY, CA, CH, CN, CR, CU, CZ, DE, DK, DM, EE, ES, FI, GB, GD, GE, GH, GM, HR, HU, ID, IL, IN, IS, JP, KE, KG, KP, KR, KZ, LC, LK, LR, LS, LT, LU, LV, MD, MG, MK, MN, MW, MX, NO, NZ, PL, PT, RO, RU, SD, SE, SG, SI, SK, SL, TJ, TM, TR, TT, UA, UG, US, UZ, VN, YU, ZA, ZW, ARIPO patent (GH, GM, KE, LS, MW, SD, SL, SZ, UG, ZW), Eurasian patent (AM, AZ, BY, KG, KZ, MD, RU, TJ, TM), European patent (AT, BE, CH, CY, DE, DK, ES, FI, FR, GB, GR, IE, IT, LU, MC, NL, PT, SE), OAPI patent (BF, BJ, CF, CG, CI, CM, GA, GN, GW, ML, MR, NE, SN, TD, TG).

Published
With international search report.
Before the expiration of the time limit for amending the claims and to be republished in the event of the receipt of amendments.

---

(54) Title: APPLICATION OF SCATTER AND ATTENUATION CORRECTION TO EMISSION TOMOGRAPHY IMAGES USING INFERRED ANATOMY FROM ATLAS

(57) Abstract

A method of applying scatter and attenuation correction to emission tomography images of a region of interest of a patient under observation comprises the steps of aligning a three–dimensional computer model representing the density distribution within the region of interest with the emission tomography images (56, 58) and applying scatter and attenuation correction to the emission tomography images using the aligned computer model as a guide (60).
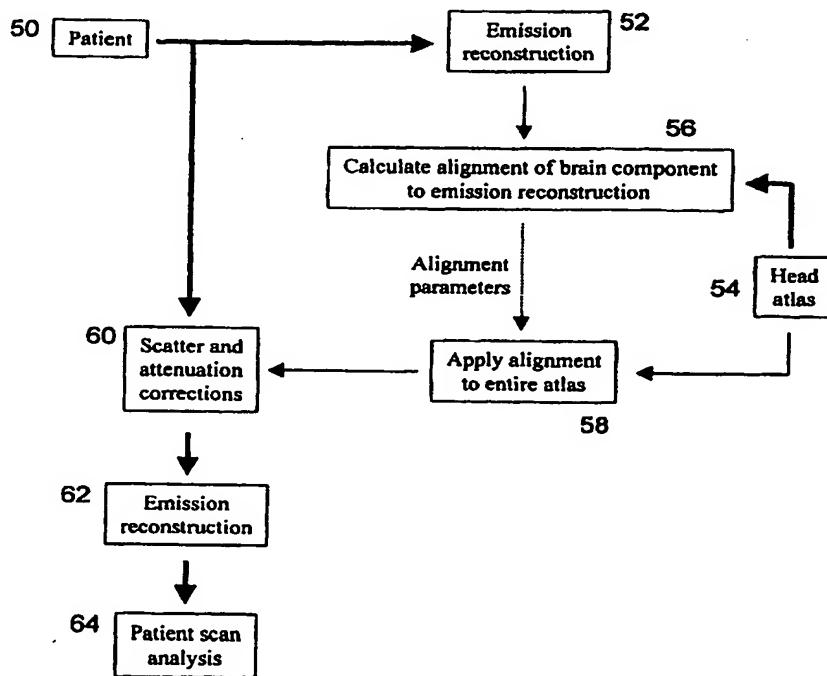
FOR THE PURPOSES OF INFORMATION ONLY

Codes used to identify States party to the PCT on the front pages of pamphlets publishing international applications under the PCT

AL	Albania	ES	Spain	LS	Lesotho	SI	Slovenia
AM	Armenia	FI	Finland	LT	Lithuania	SK	Slovakia
AT	Austria	FR	France	LU	Luxembourg	SN	Senegal
AU	Australia	GA	Gabon	LV	Latvia	SZ	Swaziland
AZ	Azerbaijan	GB	United Kingdom	MC	Monaco	TD	Chad
BA	Bosnia and Herzegovina	GE	Georgia	MD	Republic of Moldova	TG	Togo
BB	Barbados	GH	Ghana	MG	Madagascar	TJ	Tajikistan
BE	Belgium	GN	Guinea	MK	The former Yugoslav	TM	Turkmenistan
BF	Burkina Faso	GR	Greece		Republic of Macedonia	TR	Turkey
BG	Bulgaria	HU	Hungary	ML	Mali	TT	Trinidad and Tobago
BJ	Benin	IE	Ireland	MN	Mongolia	UA	Ukraine
BR	Brazil	IL	Israel	MR	Mauritania	UG	Uganda
BY	Belarus	IS	Iceland	MW	Malawi	US	United States of America
CA	Canada	IT	Italy	MX	Mexico	UZ	Uzbekistan
CF	Central African Republic	JP	Japan	NE	Niger	VN	Viet Nam
CG	Congo	KE	Kenya	NL	Netherlands	YU	Yugoslavia
CH	Switzerland	KG	Kyrgyzstan	NO	Norway	ZW	Zimbabwe
CI	Côte d'Ivoire	KP	Democratic People's	NZ	New Zealand		
CM	Cameroon		Republic of Korea	PL	Poland		
CN	China	KR	Republic of Korea	PT	Portugal		
CU	Cuba	KZ	Kazakstan	RO	Romania		
CZ	Czech Republic	LC	Saint Lucia	RU	Russian Federation		
DE	Germany	LI	Liechtenstein	SD	Sudan		
DK	Denmark	LK	Sri Lanka	SE	Sweden		
EE	Estonia	LR	Liberia	SG	Singapore		

APPLICATION OF SCATTER AND ATTENUATION CORRECTION TO EMISSION TOMOGRAPHY IMAGES USING INFERRED ANATOMY FROM ATLAS

5   **Technical Field**

The present invention relates to emission tomography and in particular to a method and apparatus for applying scatter and attenuation correction to emission tomography images using anatomy inferred from an atlas.

10   **Background Art**

Single Photon Emission Computed Tomography (SPECT) and Positron Emission Tomography (PET) are nuclear medicine diagnostic imaging techniques used to measure the three-dimensional distribution of a radiopharmaceutical within the body. Brain SPECT and PET imaging techniques are primarily used to measure regional cerebral blood

15   flow in a patient injected with a radiopharmaceutical to assist in the evaluation of stroke and the diagnosis of dementias such as Alzheimer's disease.

Although SPECT and PET are useful imaging techniques, their poor quantitative accuracy has been an obstacle in the ability to achieve increased diagnostic reliability. Quantitative accuracy of brain SPECT and PET imaging has however been

20   improved significantly through the application of scatter and attenuation correction to SPECT and PET brain images. To be sufficiently accurate, the application of scatter and attenuation correction to SPECT and PET brain images must be guided by the distribution of density within the head. Unfortunately, the distribution of density within the head cannot be obtained from SPECT and PET brain scans and therefore, separate measurements are required.

25   Transmission imaging has been used to measure the distribution of density within the head to allow scatter and attenuation correction to be applied to SPECT and PET brain images. Unfortunately, the hardware necessary for making transmission measurements is complex, unreliable and requires extensive maintenance. Also, the need to make transmission imaging measurements in addition to the SPECT or PET brain images, increases

30   the time required to complete the overall imaging procedure. SPECT and PET imaging procedures are themselves lengthy and require a patient to remain motionless to ensure accurate brain images. For sick and elderly patients, this is a difficult task. Adding to the length of the imaging procedure increases the likelihood that patients will not remain

motionless. Movement of a patient during the transmission imaging procedure results in inaccurate measurements of the distribution of density within the head. This of course provides an inaccurate guide for the application of scatter and attenuation correction to SPECT and PET brain images. Accordingly, improved methods to increase the diagnostic reliability of emission tomography images are desired.

It is therefore an object of the present invention to provide a novel method and apparatus for applying scatter and attenuation correction to emission tomography images.

Disclosure Of The Invention

Broadly stated, the present invention provides a method and apparatus for applying scatter and attenuation correction to emission tomography images which estimates or "infers" the distribution of density within a region of interest of a patient under observation using a three-dimensional computer model of the region of interest. It has been found that scatter and attenuation correction guided by a computer model of the region of interest under observation produces results similar to those when using transmission images of the actual region of interest as the guide to the application of scatter and attenuation correction.

According to one aspect of the present invention there is provided a method of applying scatter and attenuation correction to emission tomography images of a region of interest of a subject under observation comprising the steps of:

aligning a three-dimensional computer model representing the density distribution within said region of interest with said emission tomography images; and

applying scatter and attenuation correction to said emission tomography images using said aligned computer model as a guide.

In a preferred embodiment, the computer model is in the form of a two-component atlas. During the aligning step, a functional component of the atlas is firstly aligned with the emission tomography images to generate a set of spatial transformation parameters. Following this, an anatomical component of the atlas is aligned with the emission tomography images using the set of spatial transformation parameters.

The atlas may be selected from a database of atlases based on degree of registration with the emission tomography images. Alternatively, multiple atlases maybe combined to yield a resultant atlas which better registers with the emission tomography images.

According to another aspect of the present invention there is provided in an emission tomography imaging system where emission tomography images of a region of interest of a subject are taken for analysis and are corrected for scatter and attenuation, the improvement comprising:

using a three-dimensional computer model approximating the density distribution within the region of interest as a guide to the application of scatter and attenuation correction.

According to still yet another aspect of the present invention there is provided an emission tomography image processing system comprising:

memory storing emission tomography images of a region of interest of a subject;

said memory also storing at least one three-dimensional computer model of said region of interest, said computer model representing the density distribution within said region of interest; and

a processor for registering said computer model with said emission tomography images and for applying scatter and attenuation correction to said emission tomography images using said registered computer model as a guide.

According to still yet another aspect of the present invention there is provided an emission tomography imaging system comprising:

means for taking emission tomography images of a region of interest of a subject to form a three-dimensional image of said region of interest;

memory to store said emission tomography images, said memory also storing at least one three-dimensional computer model of said region of interest, said computer model representing the density distribution within said region of interest; and

a processor for aligning said computer model with said emission tomography images and for applying scatter and attenuation correction to said emission tomography images using said aligned computer model as a guide.

According to still yet another aspect of the present invention there is provided a computer readable medium including computer program code for applying scatter and attenuation correction to emission tomography images of a region of interest of a subject, said computer readable medium including:

computer program code for aligning a three-dimensional computer model representing the density distribution within said region of interest with said emission tomography images; and

computer program code for applying scatter and attenuation correction to said emission tomography images using said aligned computer model as a guide.

The present invention provides advantages in that by using a three-dimensional computer model of the region of interest of a subject under observation that approximates its density as a guide for the application of scatter and attenuation correction to emission tomography images, the need for transmission imaging is obviated. Therefore, in the case of SPECT and PET imaging, the imaging procedures do not need to be lengthened. Also, since the distribution of density in the region of interest under observation is approximated by a three-dimensional computer model, additional hardware is not required to create the guide for the application of scatter and attenuation correction. This makes the present invention significantly less expensive and more flexible than transmission imaging systems. In addition, since a three-dimensional computer model of the region of interest under observation is used as the guide for the application of scatter and attenuation correction, scatter and attenuation correction can be applied retrospectively to existing databases which include significant numbers of emission tomography images for which no transmission imaging measurements were acquired.

Brief Description Of The Drawings

An embodiment of the present invention will now be described more fully with reference to the accompanying drawings in which:

Figure 1a shows a two-dimensional emission tomography brain image without the application of scatter and attenuation correction;

Figure 1b shows the two-dimensional image of Figure 1a with the application of scatter and attenuation correction;

Figure 1c is a two-dimensional transmission brain image;

Figures 1d and 1e are two-dimensional emission tomography brain images with appurtenant anatomy derived from transmission images applied thereto;

Figure 2 is a block diagram showing a method for applying scatter and attenuation correction to emission tomography images in accordance with the present invention;

Figure 3a shows a two-dimensional emission tomography brain image of a head phantom with scatter and attenuation correction;

Figure 3b is a two-dimensional transmission brain image;

Figures 3c and 3d are two-dimensional emission tomography brain images with appurtenant anatomy derived from transmission images applied thereto;

Figures 3e and 3f are two-dimensional emission tomography brain images with inferred anatomy derived from an atlas applied thereto;

Figures 4 and 5 show two-dimensional brain images and a graph comparing uniform appurtenant anatomy, uniform inferred anatomy and brain contour;

Figure 6 shows two-dimensional brain images with non-uniform appurtenant and non-uniform inferred anatomy applied thereto;

Figures 7 and 8 show quantitative evaluation of head phantom SPECT reconstructions;

Figure 9 shows two-dimensionl SPECT brain images;.

Figure 10 shows SPECT brain images superimposed onto transmission reconstruction and inferred anatomy;

Figure 11 shows profiles taken through reconstructions of a SPECT brain image;

Figure 12 is a graph showing a comparison of regional cerebral blood flow from reconstructed SPECT images guided by inferred anatomy and transmission scans; and

Figure 13 is a graph showing the correlation between the reconstructed SPECT images of Figure 12.

Best Mode for Carrying Out The Invention

During emission tomography imaging such as for example SPECT and PET, a patient is injected with a radiopharmaceutical. Two-dimensional images or projections of a region of interest (ROI) of a patient are taken along an arbitrary axis. The projections are digitized and conveyed to a computer for storage in a three-dimensional array in computer memory to reconstruct a three-dimensional image of the region of interest. Once the three-

dimensional image is reconstructed, two-dimensional slices of the region of interest can be viewed along virtually any arbitrary axis using conventional software. Figure 1a shows a two-dimensional emission tomography brain image.

During the imaging procedure, the emissions from the radiopharmaceutical are scattered and/or attenuated by different density tissue, air cavities and/or bones in the region of interest under observation. As can be seen in Figure 1a, scattering and attenuation of radiopharmaceuticals affects quantitative image quality. As a result, acquired emission tomography images are often unreliable. Applying scatter and attenuation correction to emission tomography images, using transmission images of the same region of interest taken during the same imaging procedure, is known but suffers from the disadvantages discussed previously. Figure 1b shows the two-dimensional image of Figure 1a with scatter and attenuation correction applied using transmission images taken of the same anatomy. Figure 1c shows an example of a transmission image and Figures 1d and 1e show appurtenant anatomy (sagittal and transverse respectively) derived from the transmission images applied to emission tomography brain images.

In the present invention, a three-dimensional computer model or "atlas" of the region of interest, which provides accurate density distribution of the region of interest, is stored in a database in computer memory and is used as a guide for the application of scatter and attenuation correction to emission tomography images. In the present embodiment, the atlas includes two components, namely a functional component simulating a SPECT OR PET scan of the region of interest and an anatomical component simulating a transmission scan of the region of interest. The atlas can be created from existing transmission images or x-ray CT scans of similar regions of interest from other patients and averaged to form a suitable computer model or atlas. Multiple models for each region of interest and models for different regions of interest can be stored in the database and accessed individually during scatter and attenuation correction of emission tomography images. Since a computer model of the region of interest is used, additional hardware and procedure time is not required to apply scatter and attenuation correction to emission tomography images. An example of the application of scatter and attenuation correction to emission tomography brain images in accordance with the present invention will now be described.

Referring now to Figure 2, a block diagram illustrating the present method for applying scatter and attenuation correction to emission tomography brain images is shown.

Initially, emission tomography brain images of a patient (block 50) are acquired in a known manner. The acquired brain images are in the form of two-dimensional projections of the radiopharmaceutical distribution in the brain.

Initially, a preliminary reconstruction of the acquired brain images is performed to digitize and assemble the two-dimensional projections into a three-dimensional array in computer memory to create a three-dimensional image of the brain (block 52). An atlas of the head (the region of interest in this case) is then downloaded from the database into a datafile (block 54) and the functional component of the head atlas is identified. Once identified, the functional component of the head atlas, in this embodiment the brain component, is copied to a three-dimensional array. Following this, an alignment procedure to register spatially the brain component of the head atlas with the three-dimensional brain image is performed (block 56). In the present embodiment, a simplex algorithm is used to register spatially, the brain component of the head atlas with the brain image as described in "Numerical Recipes In C" by Press et al, 2nd edition, New York, New York, Cambridge University Press, 1992. Those of skill in the art will however appreciate that other registration algorithms can be used to align the brain component of the head atlas to the three-dimensional brain image. During this alignment procedure, a set of 3D spatial transformation parameters representing the three-dimensional transformations, including but not limited to rotation, shifting and scaling, that are necessary to register the brain component of the head atlas with the three-dimensional brain image, is calculated and is stored in the computer memory as a matrix.

Once the set of 3D transformation parameters is calculated and stored, the 3D spatial transformation parameters in the set are applied to the anatomical component of the head atlas to register it with the three-dimensional brain image (block 58). With the anatomical component of the head atlas aligned with the three-dimensional brain image, the atlas can be used as a density distribution guide to the application of scatter and attenuation correction to the three-dimensional brain image.

With an accurate density distribution guide established, scatter correction is applied to the three-dimensional brain image followed by attenuation correction in a known manner (block 60). Once scatter and attenuation correction has been applied to the three-dimensional brain image, the brain image is reconstructed into a three-dimensional array in computer memory to complete the image correction process (block 62). The corrected three-

dimensional brain image can then be analyzed (block 64). Appendix A includes pseudocode representing the above-identified process.

Figures 3a to 3f show a comparison of two-dimensional brain images of a head phantom with anatomy derived from transmission images (appurtenant anatomy) and anatomy derived from a head atlas (inferred anatomy) applied.

The present method and apparatus was tested using an anthropomorphic head phantom modeling soft tissue, hard tissue and air cavities within a skull and including a two-compartment brain reservoir. The two compartments of the reservoir were separately filled with two water solutions of Tc-99m, having a specific activity ratio of 4:1. Fan-beam SPECT was acquired followed by a Tc-99m transmission scan sixty hours later. The reconstructed transmission image is referred to as appurtenant anatomy.

Five scatter and attenuation correction schemes were evaluated based on non-uniform appurtenant anatomy, uniform appurtenant anatomy, non-uniform inferred anatomy, uniform inferred anatomy, and uniform brain contour. For uniform scatter and attenuation correction, the inferred and appurtenant anatomies were segmented and assigned uniform attenuation coefficients of soft tissue ($0.15cm^{-1}$ for Tc-99m). A SPECT reconstruction of the head phantom was similarly processed to facilitate scatter and attenuation correction guided by brain contour. Scatter correction was based on a non-stationary deconvolution scatter subtraction as described in the paper authored by Stodilka et al entitled "The Relative Contributions of Scatter and Attenuation Correction Toward Brain SPECT Quantification", Phys Med Biol, 1998. Attenuation correction/reconstruction was subsequently performed by ordered-subsets expectation-maximization as set out in the paper authored by Hudson HM et al entitled "Accelerated Image Reconstruction using Ordered Subsets of Projection Data", *IEEE Trans Med Imaging* 13 601-609, 1994. Although particular examples of scatter correction, attenuation correction and reconstruction algorithms are described, those of skill in the art will appreciate that other scatter correction, attenuation correction and reconstruction methods can be used.

Uniform scatter and attenuation correction should be guided by the contour of the attenuating medium if an acceptable level of accuracy for objective diagnosis is to be expected. Figures 4 and 5 show that uniform appurtenant anatomy is better approximated by uniform inferred anatomy than by brain contour. As can be seen in Figure 6, non-uniform appurtenant anatomy and non-uniform inferred anatomy are similar.

Head phantom SPECT reconstructions were quantitatively evaluated by four metrics, namely bias, uniformity, contrast-recovery, and relative quantification (see Figures 7 and 8). As will be appreciated, scatter and attenuation correction guided by inferred anatomy provides quantitative accuracy that is distinctively superior to scatter and attenuation correction guided by brain contour.

Application of scatter and attenuation correction to emission tomography images of anatomy other than the head can also be performed. For example, inferred anatomy can also be used to apply scatter and attenuation correction to cardiac images. During construction of the cardiac atlas, an anatomical component of the cardiac atlas representing the anatomical features of the thorax is created and includes:

soft-tissues such as the heart, liver, muscle, and fat;

very low-density soft-tissues such as the lungs; and

high-density tissues such as bone and cartilage in the ribs and spine.

A functional component of the cardiac atlas is also created and simulates a SPECT or PET cardiac image. Appropriate data to construct the cardiac atlas can be obtained in a variety of ways including, but not limited to, imaging a phantom or human subject by X-ray CT, MRI, or gamma-camera transmission computed tomography; or computer simulation. Also, the cardiac atlas can be constructed by amalgamating a plurality of patient scans.

The procedure of using inferred cardiac anatomy to apply scatter and attenuation correction to cardiac images remains the same as with brain imaging described above. First, a preliminary reconstruction of the patient's cardiac SPECT data is performed. The functional component of the cardiac atlas is then registered to the preliminary reconstruction. The registration includes a spatial transformation that may include shifting, rotation, scaling, and/or non-linear operations such as warping. The registration procedure calculates a matrix representing the spatial transformation that maps atlas space into patient-specific space. Once the matrix has been calculated, the matrix is applied to the anatomical component of the cardiac atlas, thus inferring anatomy in the chest.

Although the above methods describe the use of a single generic atlas of the anatomy under observation, those of skill in the art will appreciate that custom atlases can be developed and stored in the database. For example, disease specific atlases such as an Alzheimer's disease atlas or a stroke atlas can be developed and used when correcting

emission tomography images of patients suffering from those diseases. The disease specific atlases may be tracer or lesion specific to allow for local concavities in radiopharmaceutical uptake. Patients with severe Alzheimer's or Pick's disease do not have normal cerebral blood flow. Areas with flow deficits can limit the accuracy of the registration of the emission tomography images with the functional component of the head atlas if the head atlas assumes normal blood flow and hence uniform radiopharmaceutcial uptake. Atlases can also be developed to take into account physical traits such as for example, an exceptionally large nasal sinus. During scatter and attenuation correction, the operator can select the appropriate atlas to use. Alternatively, the atlas can be selected automatically by computer software. In this case, the software, performs a preliminary reconstruction using each custom atlas and registers the atlas to the preliminary reconstruction to measure the accuracy of the registration. The atlas with the highest registration accuracy is then selected. If desired, the software can use fuzzy logic, theoretical calculations or other criteria to combine two or more atlases to yield a single resultant atlas, which provides a better degree of registration.

EXAMPLE

Example 1: Inferred Anatomy and Brain Imaging

The following example is described for the purposes of illustration and is not intended to limit the scope of the present invention.

Inferring Anatomy From A Head Atlas

A head atlas was prepared as follows. A Zubal three-dimensional digitized MRI head phantom [Zubal *et al* 1994] was segmented to produce two data sets, namely a SPECT atlas simulating a SPECT scan of the phantom, and an anatomical atlas simulating a transmission scan of the phantom. The SPECT atlas consisted of voxels containing gray-matter and white-matter, to which ^{99m}Tc-HMPAO relative uptakes of 4 and 1 had been assigned respectively. The anatomical atlas consisted of voxels containing hard-tissue, soft-tissue and nasal sinus, to which the correspondent 140keV narrow-beam attenuation coefficients of 0.25, 0.15, and 0.075 cm^{-1} were assigned.

A patient SPECT scan was then reconstructed without scatter and attenuation correction. Facial activity was removed to yield a data set referred to as the preliminary patient reconstruction. The SPECT atlas was then registered to the preliminary patient reconstruction and the spatial transformation was recorded. This transformation was then applied to the anatomical atlas, thus inferring the location of the patient's soft-tissue, hard-tissue and air cavities (see Figure 9).

A general-purpose radiological analysis program (Hermes, Nuclear Diagnostics, Stockholm, Sweden) was used to perform the unimodality registration. The large variation in head orientation necessitated that a manual registration be first performed. This was followed by an automated refinement. The cost function of the automated registration was defined as the sum of absolute count differences [Hoh *et al* 1993]. A global minimum was sought by a simplex search [Nelder and Mead 1965] within a parameter space consisting of rotating, shifting, and linear scaling in x, y, and z directions [Holman *et al* 1991, Slomka *et al* 1995].

Sequential Transmission And Emission Imaging

Ten dementia patients (5 females and 5 males, with a mean age of 64.3 years) were analyzed. For each patient, a transmission scan was first acquired. Patients became very relaxed during the quiet transmission scan, and were then injected with 740 MBq of ^{99m}Tc-HMPAO. The SPECT procedure was started approximately 5 minutes post-injection. The SPECT system, which has transmission capabilities, is described in detail [Kemp *et al* 1995]. It consists of a General Electric 400AC/T gamma camera (General Electric, Milwaukee, WI) with a 409.6 mm diameter circular field-of-view. Projections were acquired through a fan-beam collimator (Nuclear Fields, Des Plaines, IL) having a 600 mm focal length and 1.5 mm flat-to-flat hexagonal hole width. The transmission component includes a frame mounted onto the camera's collimator that holds a tantalum-collimated ^{99m}Tc line source along the focal line of the fan-beam collimator. Collimation of both the line source and camera minimizes scatter. As a result, the transmission system effectively measures narrow-beam attenuation coefficients [Tsui *et al* 1989, Kemp *et al* 1995]. SPECT and transmission scans were acquired with a 20% energy window, centered on the ^{99m}Tc photopeak of 140 keV. The scans consisted of 128 projections, equally spaced over 360°. Each circular projection was acquired into a 128 x 128 pixel square matrix (1 pixel = 3.2

mm). Both transmission and SPECT scans were 10 seconds per projection and count rates were approximately 70 and 1.5 kcounts per second, respectively. All scans were corrected for uniformity using 100 million count flood images, and transmission scans were normalized to 50 million count blank images. Radii of rotation varied among the patients; the smallest being 170 mm and the largest being 205 mm. Prior to reconstruction, all scans were rebinned to object-plane parallel-hole geometry via two-dimensional cubic interpolation.

Scatter And Attenuation Correction And Reconstruction

The SPECT data were reconstructed using a maximum-likelihood estimator with an unregularized 32-level ordered subset [Hudson and Larkin 1994] implementation of the expectation maximization algorithm [Shepp and Vardi 1982, Lange and Carson 1984] (OSEM). The four projections that were used per sub-iteration were equally spaced about 360°. Attenuation was modelled in the matched projector/backprojector pair, and a scatter estimate [Stodilka et al 1998b] was added as an a priori background following forward projection [Lange and Carson 1984, Bowsher et al 1996, Kadrmas et al 1998]. Both scatter and attenuation modelling incorporated the narrow-beam attenuation coefficients from transmission imaging or inferred anatomy. Detector response was not included. Four iterations of OSEM were used, following initialization with a uniform [Nunez and Llacer 1990] support prior derived from transmission reconstruction or inferred anatomy. Reconstructions were then post-filtered [Nunez and Llacer 1990] using a three-dimensional Butterworth filter with an order of 8 and cutoff at 0.42 cm^{-1}. The transmission data were also reconstructed by the emission OSEM algorithm, following blank scan normalization and log-transformation.

Line source collimation, coupled with limitations in detector count rate capability and patient compliance resulted in less than ideal transmission statistics. To reduce the effects of transmission imaging noise propagation into the SPECT reconstruction [Xu et al 1991, Tung and Gullberg 1994], the transmission reconstructions were segmented as follows. Soft-tissue in the reconstructed transmission volumes was forced to have uniform density. First, a large region of interest (ROI) was drawn around soft-tissue regions, and mean and variance estimates were calculated. Then, all voxels having count densities within ±2 standard deviations of this mean were assigned to 0.15cm^{-1}. Thus, the transmission

reconstructions were characterized by noiseless soft-tissue, yet featured hard-tissue and air cavities.

Template-Based Quantification

Previous work has identified that a major confound to reproducible quantification, originates from manual and threshold-dependent placement of anatomical ROIs onto SPECT scans [Msaki *et al* 1998]. To reduce this subjective source of error, a normal template [Msaki *et al* 1998] onto which twelve bilateral volumetric ROIs are demarcated [Karbe *et al* 1994] was used. The ability to store the template and its ROIs ensures reproducibility of the analysis. This quantification procedure also introduces standardization to the analysis, which facilitates the exchange of data among different institutions [Evans *et al* 1988]. All reconstructed scans were registered to the normal template, herein referred to as "spatial normalization". Prior to spatial normalization, voxels previously identified as facial activity were set to zero. Following superposition of the template ROIs onto each scan, the cortical rCBF for each ROI was normalized to cerebellar rCBF [Karbe *et al* 1994] and corrected for blood flow-dependent tracer reflux [Lassen *et al* 1988]. Analysis of the absolute concentration of radiopharmaceutical was not performed since currently, absolute rCBF quantification is seldom used in SPECT [Bakker and Pauwels 1997].

Quantitative Error Analysis

A sample of inferred anatomy and transmission reconstruction is illustrated in Figure 10. In Figure 11, profiles through the SPECT reconstructions guided by transmission scans and inferred anatomy are presented. The profiles have not been normalized to cerebellar count density.

The means and standard errors of regional cerebral blood flow from SPECT scans guided by inferred anatomy and transmission scans were compared ROI-by-ROI (see Figure 12). Statistical analysis was also performed ROI-by-ROI using repeated analysis of variance to determine where there were significant differences between the inferred anatomy versus transmission-guided reconstruction methods. Pooled-ROI and ROI-dependent correlation coefficients were calculated between inferred anatomy reconstruction and transmission-guided SPECT reconstructions. Figure 13 shows the correlation between the

two reconstruction and quantification methods by pooling all ROIs and patients together. The p value for significance was set to 0.05 for all tests.

Inferred Anatomy Error Propagation Analysis

Four sources of error were identified that contribute to discrepancies in ROI quantification:

(1) inferred anatomy-guided scatter correction;

(2) inferred anatomy-guided attenuation correction;

(3) inferred anatomy-guided spatial normalization, which is equivalent to ROI misplacement; and

(4) patient motion between transmission and SPECT scans.

The first two are inherent limitations to the principle of inferred anatomy, whereas the last two represent artifactual exaggerations of errors in the context of this example. The first three sources of error, namely scatter, attenuation, and ROI misplacement were measured.

The propagation of ROI quantification to differences between inferred anatomy scatter correction and transmission-guided scatter correction were analyzed by performing:

(1) inferred anatomy-derived scatter correction;

(2) transmission-derived attenuation correction; and

(3) applying the spatial normalization calculated to be optimal for registering the transmission-derived SPECT reconstruction to the quantification template.

A similar analysis for evaluating the effects of inferred anatomy-derived attenuation correction was carried out by performing:

. (1) transmission –derived scatter correction;

(2) inferred-anatomy derived attenuation correction; and

(3) applying the spatial normalization calculated to be optimal for registering the transmission-derived SPECT reconstruction to the quantification template.

The effects of ROI misplacement were quantified by performing transmission-derived scatter and attenuation correction, and then applying the spatial transformation calculated to be optimal for registering the inferred anatomy-derived SPECT reconstruction to the quantification template. Thus, the full propagation analysis resulted in three reconstructions, each of which was quantitatively compared (via the above-described template-based quantification procedure) with the "gold-standard" transmission-derived SPECT reconstruction and spatial normalization. This procedure was performed for the ten patients, and the results averaged. However, once the errors due to scatter, attenuation, and ROI misplacement were separately quantified, their totals were found to be less than the errors caused by the full inferred anatomy protocol. This additional source of error is termed "unaccountable" in Table 2, and is believed to be caused by patient motion.

Qualitative Analysis

A sample comparison of inferred anatomy and transmission reconstruction is shown in Figure 10 for mid-sagittal and cortical-axial slices. Good reproduction of soft-tissue and hard-tissue at the cortical level is noted. Some discrepancy is seen near the vertex; however, this region is seldom included in quantitative analysis. Discrepancies near the nasal sinus are most marked. Fortunately, these structures mostly involve low-density areas such as air, and to a much lesser degree, soft-tissues and cartilage, which do not scatter and attenuate photons as much as higher density structures.

Mid-brain profiles, shown in Figure 11, compare a SPECT reconstruction guided by transmission imaging with the same SPECT reconstruction guided by inferred anatomy. The profile was taken along the longest axis of the head, which is most sensitive to mis-registered transmission maps following scatter and attenuation correction [Huang et al 1979].

Quantitative Error Analysis

Table 1 below shows the results of the repeated analysis of variance and correlation analysis comparing transmission reconstruction and quantitative and inferred anatomy-guided reconstruction and quantification. Left frontal and central sulcus ROIs showed the highest probability of a true difference, reaching statistical significance with p=0.001 and 0.002, respectively. These ROIs also had the highest correlation coefficients

relating transmission reconstruction and quantification and inferred anatomy-guided SPECT reconstruction and quantification. This increased correlation may be an artifact of the increased differences in the ROI means. Interestingly, the left frontal and central sulcus ROIs were also found to have marked rCBF deficits, suggesting that inferred anatomy may have difficulties near regions with substantially reduced radiopharmaceutical uptake.

Figure 12 shows the means and standard errors for transmission reconstruction and inferred anatomy in each of the 12 ROIs, averaged across the entire population. The mean absolute difference for all ROIs across the whole population was 7.5%. Correlation for all ROIs and all patients was found to be high: $r^2=0.92$ as illustrated in Figure 13.

TABLE 1

Region	ANOVA Significance	Paired sample correlation	Paired sample Significance
Left frontal	0.001	0.965	<0.001
Right frontal	0.088	0.953	<0.001
Left central sulcus	0.002	0.957	<0.001
Right central sulcus	0.234	0.937	<0.001
Left parietal	0.092	0.772	0.009
Right parietal	0.473	0.862	0.001
Left temporal	0.957	0.939	<0.001
Right temporal	0.397	0.835	0.003
Left occipital	0.271	0.835	0.003
Right occipital	0.073	0.858	0.001
Left cerebellar	0.545	0.938	<0.001
Right cerebellar	0.603	0.925	<0.001

Error Propagation Analysis

The results from the propagation analysis are presented in Table 2 below. These results are presented as errors relative to the "gold-standard" transmission reconstruction-guided reconstruction and spatial normalization. Three sources of error due to inferring anatomy were analyzed namely, errors in scatter distribution estimates, errors due to misguided attenuation compensation, and errors due to region-of-interest misplacement. The error components, averaged across ten patients, are shown for each of the twelve bilateral regions-of-interest. The table summarizes the percentage that each of these error sources contributed to the total quantitative differences between SPECT reconstructions guided by transmission scans or inferred anatomy. The fourth numerical column indicates the percentage of total differences that could not be accounted for by inferring anatomy.

On average, it was found that errors in scatter distribution estimates results in approximately 10.0% of the total quantitative error; attenuation correction: 36.6%, and ROI misplacement: 27.0%. The relative contributions of inferred anatomy-derived scatter and attenuation correction to the total error seem credible. Compensating for attenuation is of considerably greater consequence than removing scattered photons [Rosenthal *et al* 1995]. Approximately 26.5% of the total discrepancy between inferred anatomy and transmission imaging could not be accounted for in the error propagation analysis of scatter, attenuation, and ROI misplacement but is belived to be as a result of patient motion during data acquisition.

TABLE 2

Region	Scatter correction %	Attenuation correction %	Region misplacement %	Unaccountable error %
Left frontal	6.1	44.5	28.6	20.8
Right frontal	12.0	49.9	29.4	8.7
Left central sulcus	5.7	40.4	17.9	36.0
Right central sulcus	6.3	34.3	16.0	43.4
Left parietal	7.9	25.7	30.3	36.1
Right parietal	10.0	34.1	25.9	30.0
Left temporal	10.0	38.3	20.0	31.8
Right temporal	13.8	27.0	30.7	28.5
Left occipital	13.2	23.2	27.6	36.0
Right occipital	8.3	22.5	29.0	40.2
Left cerebellar	13.5	48.7	31.9	5.8
Right cerebellar	12.5	50.2	36.4	0.8
Average	**10.0**	**36.6**	**27.0**	**26.5**

Qualitative and Quantitative Comparisons

Comparing inferred anatomy with transmission reconstructions indicated good reproduction of soft-tissue and hard-tissue in cortical areas for all ten patients. However, in many scans, a discrepancy was indicated near the sinus cavity, as shown in Figure 10. Despite this, inferred anatomy is more robust and accurate in providing estimates of underlying tissue distribution than fitting ellipses to photopeak emission data. The technique of fitting ellipses depends on adequate facial activity since the contours of the brain and head differ so considerably at the level of the cerebellum. Facial activity should not form the basis for estimating underlying tissue distributions since uptake varies with radiopharmaceutical and time between injection and scanning [Leveille *et al* 1992, Van Dyck *et al* 1996], making

it an unreliable dependency. Parenthetically, the qualitative similarities demonstrated between inferred anatomy and transmission reconstruction indicate confidence in accurately guiding scatter and attenuation correction. However, it is important to note that similar shape is a sufficient, but not necessary, prerequisite for accurate scatter and attenuation correction [Welch *et al* 1997, Natterer 1993].

Slight truncation effects are noticed on the transmission images for three of the ten scans. Truncation occurred for kyphotic patients with broad shoulders or with short necks. This limitation was generally restricted to transaxial slices below the level of the cerebellum or very near its base, where the gamma camera's circular field-of-view proved to be inconvenient. The truncation only involved nasal cartilage, and is therefore not expected to significantly impact results, as is demonstrated in the quantitative accuracy exhibited at the cerebellar level (see Figure 12).

Inferred anatomy had difficulties in regions with marked rCBF deficit, such as the left frontal lobe. Although frontal lobes generally exhibit high variability in HMPAO uptake [Deutsch *et al* 1997], only the left frontal lobe had statistically significant error. This suggests that regional quantitative errors incurred by inferred anatomy are associated with rCBF deficits. However, previous work demonstrates that they may also be sensitive to spatial region. Achieving good quantitative accuracy in extended sources is often difficult and this is particularly true with peripheral ROIs, where reconstructed activity is most sensitive to misregistration of the attenuating medium [Huang *et al* 1979]. For example, in the brain a mismatch between emission and transmission data no greater than 5mm can produce a 10% error in a 10 mm thick peripheral cortical ROI [Andersson *et al* 1995b, Huang *et al* 1979]. In general, extended sources, such as the brain, are affected by misregistration more than compact sources, such as the heart [Andersson *et al* 1995b, McCord *et al* 1992, Ter-Pogossian 1992, Matsunari *et al* 1998]. Since the brain is elliptical, it is expected that regions along the periphery of the long axis of the head will be more sensitive to attenuation map misregistration than those along the short axis.

Although a preferred embodiment of the present invention has been described, those of skill in the art will appreciate that variations and modifications may be made to the

present invention without departing from the spirit and scope thereof as defined by the appended claims.

APPENDIX A

```
emis_proj =          //initialize 3D array. Projections are 2D, but we have
                     //many projections.

emis_proj_sc =       //init 3D array. Store projections here after scatter
                     //correction.

emis_proj_sc_ac =    //init 3D array. Store projections here after scatter and
                     //attenuation correction.

emis_reco_sc_ac =    //init 3D array. The reconstructed 3D brain scan.

tx_proj =            //init 3D array. Transmission projections of anatomy.

anatomy =            //init 3D array. The 3D distribution of anatomy goes
                     //here.



emis_proj = do_patient_emission_scan;
                     // first step is to acquire the patient emission scan.
                     // The acquire data is in the form of projections of the
                     // radiopharmaceutical distribution.

                     // These projections require scatter and attenuation
                     // correction.
                     // In order to perform these corrections, an estimate of
                     // anatomy must be obtained. Current, two methods of
                     // obtaining an anatomy estimate are possible:
if (infer==1)
        anatomy = infer_anatomy(emis_proj); // This is our method. See the
                                            // function, below. This is what
                                            // we are patenting.

elseif (infer==0)
{
                     // Alternatively, we acquire transmission projections of
                     // the patient.
                     // This is very similar to x-ray CT.
        tx_proj = do_patient_transmission_scan;
```

APPENDIX A

```
anatomy = reconstruct(tx_proj);        // These projections are
                                       // reconstructed into a 3D
                                       // distribution of anatomy. Note
                                       // that this reconstruction is
                                       // almost identical to the
                                       // emission reconstruction;
                                       // however, transmission
                                       // reconstructions do not
                                       // require scatter or attenuation
                                       // correction.

}


                 // After we have our emission projections and an anatomy
                 // estimate, we sequentially apply scatter correction and
                 // attenuation correction to the emission data.


emis_proj_sc = scatter_correction(emis_proj,anatomy);
                         // Perform the scatter correction on the
                         // emission_data.
                         // The scatter correction requires knowing the
                         // anatomy.

emis_proj_sc_ac = attenuation_correction(emis_proj_sc,anatomy);
                         // Perform the attenuation correction on the
                         // emission data that has been scatter corrected.
                         // The attenuation correction requires knowing the
                         // anatomy.

emis_reco_sc_ac = reconstruct(emis_proj_sc_ac);
                         // After correcting the emission data for scatter
                         // and attenuation, perform the emission
                         // reconstruction.
Stop
```

APPENDIX A

```
function aligned_head_atlas = infer_anatomy(emis_proj);
{
        emis_reco =    // init 3D array. This will hold a preliminary emission
                       // reconstruction that has NOT been corrected for scatter
                       // or attenuation.

        head_atlas =        // init 3D array. This will hold the full head
                            // atlas (brain, skull, soft tissue). The head
                            // atlas is in its original orientation.

        head_atlas_brain =      // init 3D array. This will hold the brain
                                // component of the head atlas. This brain
                                // component will be in its original
                                // orientation.

        alignment_par =    // a set of parameters that represent the 3D
                           // transformations (including, but not limited to:
                           // rotation, shifting, scaling) necessary to align
                           // head_atlas_brain to emis_reco. These
                           // transformations will be applied to head_atlas.

        aligned_head_atlas =    // init 3D array. The alignment parameters
                                // are applied to head_atlas. This variable
                                // is the function's output.



        emis_reco = reconstruct(emis_proj)    // Perform a preliminary
                                              // reconstruction of the emission
                                              // data.
```

APPENDIX A

```
head_atlas = load_3D_data(atlas_filename);          // Load the head
                                                    // atlas.
head_atlas_brain = extract(head_atlas,brain);       // Identify and
                                                    // extract the brain
                                                    // from the head
                                                    // atlas.
alignment_par = find_optimal_alignment(emis_reco,head_atlas_brain);
                        // Calculate the 3D transformation parameters
                        // to align head_atlas_brain to emis_reco.
                        // This procedure calculates the optimal set
                        // of transformation parameters. In medical
                        // science, this alignment is known as
                        // "registration".
aligned_head_atlas = apply_alignment(head_atlas,alignment_par);
                        // Apply the alignment to head_atlas.
                        // aligned_head_atlas
                        // represents an anatomy estimate that is
                        // used for guiding the scatter and
                        // attenuation corrections. (Note that the
                        // variable aligned_head_atlas is passed back
                        // as anatomy to the main program.) Also note
                        // that, although the set of transformation
                        // parameters that was calculated represents
                        // the optimal set for aligning
                        // head_atlas_brain to emis_reco, these same
                        // parameters are now applied to head_atlas.
}
```

-24-

REFERENCES.

1. Acton PD and Friston KJ (1998) Statistical parametric mapping in functional neuroimaging: beyond PET and fMRI activation studies *Eur J Nucl Med* **25** 663-667

2. Andersson JLR, Sundin A and Valind S (1995a) A Method for Coregistration of PET and MR Brain Images *J Nucl Med* **36** 1307-1315

3. Andersson JLR, Vagnhammer BE and Schneider H (1995b) Accurate Attenuation Correction Despite Movement during PET Imaging *J Nucl Med* **36** 670-678

4. Andersson JLR (1995c) A Rapid and Accurate Method to Realign PET Scans Utilizing Image Edge Information *J Nucl Med* **36** 657-669

5. Ardekani B, Braun M and Hutton B (1993) Improved quantification with the use of anatomical information in PET image reconstruction. In: Uemura K, Lassen NA, Jones T, Kanno I, eds. *Quantification of Brain Function, tracer kinetics and image analysis in brain PET.* International congress series no **1030** 351-359

6. Ashare AB and Chakraborty DP (1994) Artificial Neural Networks: Better Than the Real Thing? *J Nucl Med* **35** 2048-2049

7. Bacharach SL and Buvat I (1995) Attenuation correction in cardiac positron emission tomography and single-photon emission computed tomography *J Nucl Cardiol* **2** 246-255

8. Bailey DL (1998) Transmission scanning in emission tomography *Eur J Nucl Med* **25** 774-787

9. Bakker D and Pauwels EKJ (1997) Stroke: the role of functional imaging *Eur J Nucl Med* **24** 2-5

10. Bergstrom M, Litton J, Eriksson L, Bohm C and Blomkvist G (1982) Determination of Object Contour from Projections for Attenuation Correction in Cranial Positron Emission Tomography *J Comp Assist Tomo* **6** 365-372

11. Bergstrom M, Eriksson L, Bohm C, Blomqvist G and Litton J (1983) Correction for Scatter Radiation in a Ring Detector Positron Camera by Integral Transformation of the Projection *J Comput Assist Tomo* **7** 42-50

12. Bailey DL, Hutton BF and Walker PJ (1987) Improved SPECT using simultaneous emission and transmission tomography. *J Nucl Med* **28** 844-851

13. Bowsher JE, Johnson VA, Turkington TG, Jaszczak RJ, Floyd CE and Coleman RE (1996) Bayesian Reconstruction and use of Anatomical A Priori Information for Emission Tomography *IEEE Trans Med Imag* **15** 673-686

14. Budinger TF and Gullberg GT (1977) Transverse section reconstruction of gamma-ray emitting radionuclides in patients. In: Ter-Pogossian MM, Phelps ME, Brownell GL, eds *Reconstruction tomography in diagnostic radiology and nuclear medicine* Baltimore: University Park Press 315-342

15. Chabriat H, Lavasseur M, Vidailhet M, Loc'h C, Maziere B, Bourguignon MH, Bonnet AM, Zilbovicius M, Raynaud C, Agid Y, Syrota A and Samson Y (1992) In-Vivo SPECT Imaging of D2 Receptor with Iodine-Iodolisuride: Results in Supranuclear Palsy *J Nucl Med* **33** 1481-1485

16. Chan KH, Johnson KA, Becker JA, Satlin A, Mendelson J, Garada B, and Holman BL (1994) A Neural Network Classifier for Cerebral Perfusion Imaging *J Nucl Med* **35** 771-774

17. Claus JJ, van Harskamp F, Breteler MMB, Krenning EP, van der Cammen TJM, Hofman A and Hasan D (1994) Assessment of cerebral perfusion with single-photon emission tomography in normal subjects and in patients with Alzheimer's disease: effects of region of interest selection. *Eur J Nucl Med* **21** 1044-1051

18. DeFigueiredo RJP, Shankle WR, Maccato A, Dick MB, Mundkur P, Mena I and Cotman CW (1995) Neural-network-based classification of cognitively normal, demented, Alzheimer disease and vascular dementia from single photon emission with computed tomography image data from brain *Proc Natl Acad Sci USA* **92** 5530-5534

19. Deutsch G, Mountz JM, Katholi CR, Liu HG and Harrell LE (1997) Regional Stability of Cerebral Blood Flow Measured by Repeated Technetium-99m-HMPAO SPECT: Implications for the Study of State-Dependent Change *J Nucl Med* **38** 6-13

20. Eberl S, Kanno I, Fulton RR, Ryan A, Hutton BF and Fulham MJ (1996) Automated Interstudy Image Registration Technique for SPECT and PET *J Nucl Med* **37** 137-145

21. Evans AC, Beil C, Marrett S, Thompson CJ and Hakim A (1988) Anatomical-Functional Correlation Using an Adjustable MRI-Based Region of Interest Atlas with Positron Emission Tomography *J Cereb Blood Flow Metab* **8** 513-530

22. Floyd CE, Jaszczak RJ, Greer KL and Coleman RE (1985) Deconvolution of Compton Scatter in SPECT *J Nucl Med* **26** 406-408

23. Frey EC, Tsui BMW and Perry JR (1992) Simultaneous acquisition of emission and transmission data for improved Tl-201 cardiac SPECT imaging using a Tc-99m transmission source. J Nucl Med **33** 2238-2245

24. Hoh CK, Dahlbom M, Harris G, Choi Y, Hawkins RA, Phelps ME and Maddahi J (1993) Automated iterative three-dimensional registration of positron emission tomography images *J Nucl Med* **34** 2009-2018

25. Hollinger EF, Loncaric S, Yu D-C, Ali A and Chang W (1998) Using Fast Sequential Asymmetric Fanbeam Transmission CT for Attenuation Correction of Cardiac SPECT Imaging *J Nucl Med* **39** 1335-1344

26. Holman BL, Zimmerman RE, Johnson KA, Carvalho PA, Schwartz RB, Loeffler JS, Alexander E, Pelizzari CA and Chen GTY (1991) Computer-Assisted Superimposition of Magnetic Resonance and High-Resolution Technetium-99m-HMPAO and Thallium-201 SPECT Images of the Brain *J Nucl Med* **32** 1478-1484

27. Hosoba M, Wani H, Toyama H, Murata H and Tanaka E (1986) Automated Body Contour Detection in SPECT: Effects on Quantitative Studies *J Nucl Med* **27** 1184-1191

28. Huang S-C, Hoffman EJ, Phelps ME and Kuhl DE (1979) Quantitation in Positron Emission Computed Tomography: 2. Effects of Inaccurate Attenuation Correction *J Comp Assist Tomo* **3** 804-814

29. Huang S-C, Carson RE, Phelps ME, Hoffman EJ, Schelbert HR, and Kuhl DE (1981) A Boundary Method for Attenuation Correction in Positron Computed Tomography *J Nucl Med* **22** 627-637

30. Hudson HM and Larkin RS (1994) Accelerated Image Reconstruction using Ordered Subsets of Projection Data *IEEE Trans Med Imag* **13** 601-609

31. Iida H, Narita Y, Kado H, Kashikura A, Sugawara S, Shoji Y, Kinoshita T, Ogawa T and Eberl S (1998) Effects of Scatter and Attenuation Correction on Quantitative Assessment of Regional Cerebral Blood Flow with SPECT *J Nucl Med* **39** 181-189

32. Jaszczak RJ, Chang L-T, Stein NA and Moore FE (1979) Whole-body Single-photon Emission Computed Tomography using Dual, Large-field-of-view Scintillation Cameras *Phys Med Biol* **24** 1123-1143

33. Juni J (1994) Taking Brain SPECT Seriously: Reflections on Recent Clinical Reports in The Journal of Nuclear Medicine *J Nucl Med* **35** 1891-1895

34. Kadrmas DJ, Frey EC and Tsui BMW (1997) Analysis of the Reconstructibility and Noise Properties of Scatter Photons in ^{99m}Tc SPECT *Phys Med Biol* **42** 2493-2516

35. Kadrmas DJ, Frey EC, Karimi SS and Tsui BMW (1998) Fast implementations of reconstruction-based scatter compensation in fully 3D SPECT image reconstruction *Phys Med Biol* **43** 857-873

36. Kaplan MS, Miyaoka RS, Kohlmyer SK, Haynor DR, Harrison RL and Lewellen TK (1996) Scatter and Attenuation Correction for In-111 Imaging Using Energy Spectrum Fitting *Med Phys* **23** 1277-1285

37. Karbe H, Kertesz A, Davis J, Kemp BJ, Prato FS and Nicholson RL (1994) Quantification of functional deficit in Alzheimer's disease using a computer-assisted mapping program for ^{99m}Tc-HMPAO SPECT *Neuroradiology* **36** 1-6

38. Kemp BJ, Prato FS, Nicholson RL and Reese L (1995) Transmission Computed Tomography Imaging of the Head with a SPECT System and a Collimated Line Source *J Nucl Med* **36** 328-335

39. Lange K and Carson R (1984) EM Reconstruction Algorithms for Emission and Transmission Tomography *J Comp Assist Tomo* **8** 306-316

40. Lassen NA, Anderson AR, Friberg L and Paulson OB (1988) The Retention of 99mTc-d,l-HM-PAO in the human brain after intracarotid bolus injection: a kinetic analysis *J Cereb Blood Flow Metab* **8** S13-S22

41. Leveille J, Demonceau G and Walovitch RC (1992) Intrasubject comparison between technetium-99m-ECD and technetium-99m-HMPAO in healthy human subjects *J Nucl Med* **33** 480-484

42. Licho R, Glick SJ, Xia W, Pan T-S, Penney BC and King MA (1999) Attenuation Compensation in 99mTc SPECT Brain Imaging: A Comparison of the Use of Attenuation Maps Derived from Transmission Versus Emission Data in Normal Scans *J Nucl Med* **40** 456-463.

43. Mangin JF, Frouin V, Bloch I, Bendriem B and Lopez-Krahe J (1994) Fast nonsupervised three-dimensional registration of PET and MR images of the brain *J Cereb Blood Flow Metab* **14** 749-762

44. Malko JA, Van Heertum RL, Gullberg GT and Kowalsky WP (1986) SPECT liver imaging using an iterative attenuation correction and an external flood source *J Nucl Med* **27** 701-705

45. Matsunari I, Boning G, Ziegler SI, Kosa I, Nekolla SG, Ficaro EP and Schwaiger M (1998) Effects of Misalignment Between Transmission and Emission Scans on Attenuation-Corrected Cardiac SPECT *J Nucl Med* **39** 411-416

46. McIntosh AR, Bookstein FL, Haxby JV and Grady CL (1996) Spatial Pattern Analysis of Functional Brain Images Using Partial Least Squares *Neuroimage* **3** 143-157

47. McCord ME, Bacharach SL, Bonow RO, Dilsizian V, Cuocolo A and Freedman N (1992) Misalignment Between PET Transmission and Emission Scans: Its Effects on Myocardial Imaging *J Nucl Med* **33** 1209-1214

48. Meikle SR, Dahlbom M and Cherry SR (1993) Attenuation Correction Using Count-Limited Transmission Data in Positron Emission Tomography *J Nucl Med* **34** 143-150

49. Meikle SR, Hutton BF and Bailey DL (1994) A Transmission-Dependent Method for Scatter Correction in SPECT *J Nucl Med* **35** 360-367

50. Mielke R, Pietrzyk U, Jacobs A, Fink GR, Ichimiya A, Kessler J, Herholz K and Heiss WD (1994) HMPAO SPET and FDG PET in Alzheimer's disease and vascular dementia: comparison of perfusion and metabolic pattern *Eur J Nucl Med* **21** 1052-1060

51. Minoshima S, Berger KL, Lee KS and Mintun MA (1992) An Automated Method for Rotational Correction and Centering of Three-Dimensional Functional Brain Images *J Nucl Med* **33** 1579-1585

52. Minoshima S, Koeppe RA, Frey KA and Kuhl DE (1994) Anatomic Standardization: Linear Scaling and Nonlinear Warping of Functional Brain Images *J Nucl Med* **35** 1528-1537

53. Msaki P, Prato FS, Stodilka RZ, Davis J, Kemp BJ, Kertesz A and Nicholson RL (1998) The Merits of Fully-Automated rCBF Determination in Eliminating Subjective Errors in Quantitative SPECT [Abstract] *J Nucl Med* **39** 106P

54. Natterer F (1993) Determination of tissue attenuation in emission tomography of optically dense media *Inverse Problems* **9** 731-736

55. Nelder JA and Mead R (1965) A Simplex method for function minimization *Comput J* **7** 308-313

56. Nunez J and Llacer J (1990) A Fast Bayesian Reconstruction Algorithm for Emission Tomography with Entropy Prior Converging to Feasible Images *IEEE Trans Med Imag* **9** 159-171

57. Panin VY, Zeng GL and Gullberg GT (1998) Reconstructions of Truncated Projections Using an Optimal Basis Expansion Derived from the Cross-Correlation of a "Knowledge Set" of a priori Cross-Sections *IEEE Trans Nucl Sci* **45** 2119-2125

58. Panin VY, Zeng GL and Gullberg GT (1999) Registration Problem in Attenuation Map Estimation using only Emission Data with Data Consistency Conditions [Abstract] *J Nucl Med* **40** 294P

59. Pellizari CA, Chen GTY, Spelbring DR, Weichselbaum RR and Chen C-T (1989) Accurate Three-Dimensional Registration of CT, PET, and/or MR Images of the Brain *J Comp Assist Tomo* **13** 20-26

60. Patterson JC, Early TS, Martin A, Walker MZ, Russell JM and Villanueva-Meyer H (1997) SPECT Image Analysis Using Statistical Parametric Mapping: Comparison of Technetium-99m-HMPAO and Technetium-99m-ECD *J Nucl Med* **38** 1721-1725

61. Phillips RL, London ED, Links JM and Cascella NG (1990) Program for PET Image Alignment: Effects on Calculated Differences in Cerebral Metabolic Rates for Glucose *J Nucl Med* **31** 2052-2057

62. Pietrzyk U, Herholz K, Fink G, Jacobs A, Mielke R, Slansky I, Wurker M and Heiss W-D (1994) An Interactive Technique for Three-Dimensional Image Registration: Validation for PET, SPECT, MRI and CT Brain Studies *J Nucl Med* **35** 2011-2018

63. Rosenthal MS, Cullom J, Hawkins W, Moore SC, Tsui BMW and Yester M (1995) Quantitative SPECT Imaging: A Review and Recommendations by the Focus Committee of the Society of Nuclear Medicine Computer and Instrumentation Council *J Nucl Med* **36** 1489-1513

64. Seibyl JP, Woods SW, Zoghbi SS, Baldwin RM, Dey HM, Goddard AW, Zea-Ponce Y, Zubal G, Germine M, Smith EO, Heninger GR, Charney DS, Kung HF, Alavi A, Hoffer PB and Innis RB (1992) Dynamic SPECT Imaging of Dopamine D2 Receptors in Human Subjects with Iodine-123-IBZM *J Nucl Med* **33** 1964-1971

65. Shepp LA and Vardi Y (1982) Maximum likelihood reconstruction for emission tomography *IEEE Trans Med Imag* **1** 113-122

66. Slomka PJ, Hurwitz G, Stephenson JA and Cradduck TD (1995) Automated alignment and sizing of myocardial stress and rest scans to three-dimensional normal templates using an image registration algorithm: a method for reproducible quantification *J Nucl Med* **36** 1115-1122

67. Stodilka RZ, Kemp BJ, Prato FS and Nicholson RL (1998a) Importance of Bone Attenuation in Brain SPECT Quantification *J Nucl Med* **39** 190-197

68. Stodilka RZ, Kemp BJ, Msaki P, Prato FS and Nicholson RL (1998b) The Relative Contributions of Scatter and Attenuation Corrections toward improved brain SPECT Quantification *Phys Med Biol* **43** 2991-3008

69. Stodilka RZ, Kemp BJ, Msaki P, Prato FS and Nicholson RL (1998c) Retrospective Scatter and Attenuation Correction by Inferring Anatomy from a Head Atlas *IEEE Medical Imaging Conference* [Abstract]

70. Stokking R, van Isselt JW, van Rijk PP, de Klerk JMH, Huiskes WLC, Mertens IJR, Buskens E and Viergever MA (1999) Integrated Visualization of Functional and Anatomic Brain Data: A Validation Study *J Nucl Med* **40** 311-316

71. Sugiura M, Kawashima R, Sadato N, Senda M, Kanno I, Oda K, Sato K, Yonekura Y and Fukuda H (1999) Anatomic Validation of Spatial Normalization Methods for PET *J Nucl Med* **40** 317-322

72. Talairach J, Tournoux P and Rayport M, eds (1988) *Co-planar stereotaxic atlas of the human brain. Three-dimensional proportional system: an approach to cerebral imaging* New York: Thieme Inc 1-122

73. Tan P, Bailey DL, Meikle SR, Eberl S, Fulton RR and Hutton BF (1993) A scanning line source for simultaneous emission and transmission measurements in SPECT *J Nucl Med* 34 1752-1760

74. Ter-Pogossian MM (1992) Misalignment Between PET Transmission and Emission Scans: Effect on Myocardial Imaging *J Nucl Med* 33 1214-1215

75. Tsao J, Stundzia A and Ichise M (1998) Fully Automated Establishment of Stereotaxic Image Orientation in Six Degrees of Freedom for Technetium-99m-ECD Brain SPECT *J Nucl Med* 39 503-508

76. Tsui BMW, Gullberg GT, Edgerton ER, Ballard JG, Perry JR, McCartney WH and Berg J (1989) Correction of Nonuniform Attenuation in Cardiac SPECT Imaging *J Nucl Med* 30 497-507

77. Tung C-H and Gullberg GT (1994) A simulation of emission and transmission noise propagation in cardiac SPECT imaging with nonuniform attenuation correction *Med Phys* 21 1565-1576

78. Tung C-H, Gullberg GT, Zeng GL, Christian PE, Datz FL and Morgan HT (1992) Nonuniform attenuation correction using simultaneous transmission and emission converging tomography *IEEE Trans Nucl Sci* 39 1134-1143

79. Van Dyck CH, Lin H, Smith EO, Wisniewski G, Cellar J, Robinson R, Narayan M, Bennett A, Delaney RC, Bronen RA and Hoffer PB (1996) Comparison of Technetium-99m-HMPAO and Technetium-99m-ECD Cerebral SPECT Images in Alzheimer's Disease *J Nucl Med* 37 1749-1755

80. Webb S, Flower MA, Ott RJ and Leach MO (1983) A comparison of attenuation correction methods for quantitative single photon emission computed tomography *Phys Med Biol* 28 1045-1056

81. Welch A, Clack R, Natterer F, and Gullberg GT (1997) Toward accurate attenuation correction in SPECT without transmission measurements *IEEE Trans Med Imag* 16 532-541

82. Woods K and Bowyer KW (1997) Generating ROC Curves for Artificial Neural Networks *IEEE Trans Med Imag* 16 329-337

83. Woods RP, Cherry SR and Mazziotta JC (1992) Rapid Automated Algorithm for Aligning and Reslicing PET Images *J Comp Assist Tomo* 16 620-633

84. Woods RP, Mazziotta JC and Cherry SR (1993) MRI-PET Registration with Automated Algorithm *J Comp Assist Tomo* 17 536-546

85. Xu EZ, Mullani NA, Gould KL and Anderson WL (1991) A Segmented Attenuation Correction for PET *J Nucl Med* 32 161-165

86. Zubal IG, Spencer SS, Imam K, Seibyl J, Smith EO, Wisniewski G and Hoffer PB (1995) Difference Images Calculated from Ictal and Interictal Technetium-99m-HMPAO SPECT Scans of Epilepsy *J Nucl Med* 36 684-689

87. Zubal IG, Harrell CR, Smith EO, Rattner Z, Gindi GR and Hoffer PB (1994) Computerized three-dimensional segmented human anatomy *Med Phys* **21** 299-302

What is claimed is:

1.   A method of applying scatter and attenuation correction to emission tomography images of a region of interest of a subject under observation comprising the steps of:

aligning a three-dimensional computer model representing the density distribution within said region of interest with said emission tomography images; and

applying scatter and attenuation correction to said emission tomography images using said aligned computer model as a guide.

2.   The method of claim 1 wherein said computer model is in the form of a two-component atlas.

3.   The method of claim 2 wherein during said aligning step, a functional component of said atlas is firstly aligned with said emission tomography images to generate a set of spatial transformation parameters and thereafter, the anatomical component of said atlas is aligned with said emission tomography images using said set of spatial transformation parameters.

4.   The method of claim 3 wherein said functional component simulates a SPECT or PET scan of said region of interest and wherein said anatomical component simulates a transmission scan of said region of interest.

5.   The method of claim 4 wherein said region of interest is the head and wherein said functional component is the brain component of a head atlas.

6.   The method of claim 4 wherein said region of interest is the heart, said functional component of said atlas simulating a cardiac image and said anatomical component of said atlas representing anatomical features of the thorax.

7.   The method of claim 6 wherein the anatomical features of the thorax include:

soft-tissues such as the heart, liver, muscle, and fat;

very low-density soft-tissues such as the lungs; and

high-density tissues such as bone and cartilage in the ribs and spine.

8.   The method of claim 3 further comprising the step of selecting an atlas from a database of atlases prior to performing said aligning step.

9.   The method of claim 8 wherein said selecting step is performed manually.

10.   The method of claim 8 wherein said selecting step is performed automatically based on the degree of registration of each atlas in said database with said emission tomography images.

11.   The method of claim 10 wherein the degree of registration is determined by:
          performing a preliminary reconstruction of each atlas; and
          registering the atlas to the preliminary reconstruction.

12.   The method of claim 10 further comprising the step of combining multiple atlases to yield a resultant atlas that better registers with said emission tomography images.

13.   The method of claim 8 wherein said database includes disease specific atlases, physical trait specific atlases and/or tracer or lesion specific atlases.

14.   In an emission tomography imaging system where emission tomography images of a region of interest of a subject are taken for analysis and are corrected for scatter and attenuation, the improvement comprising:
          using a three-dimensional computer model approximating the density distribution within the region of interest as a guide to the application of scatter and attenuation correction.

15.   The emission tomography imaging system of claim 14 wherein said computer model is in the form of a two-component atlas.

16.		The emission tomography imaging system of claim 15 wherein during said aligning step, a functional component of said atlas is firstly aligned with said emission tomography images to generate a set of spatial transformation parameters and thereafter, the anatomical component of said atlas is aligned with said emission tomography images using said set of spatial transformation parameters.

17.		The emission tomography imaging system of claim 16 wherein said functional component simulates a SPECT or PET scan of said region of interest and wherein said anatomical component simulates a transmission scan of said region of interest.

18.		An emission tomography image processing system comprising:
		memory storing emission tomography images of a region of interest of a subject;
		said memory also storing at least one three-dimensional computer model of said region of interest, said computer model representing the density distribution within said region of interest; and
		a processor for registering said computer model with said emission tomography images and for applying scatter and attenuation correction to said emission tomography images using said registered computer model as a guide.

19.		An emission tomography image processing system as defined in claim 18 wherein said at least one computer model is in the form of at least one two-component atlas.

20.		An emission tomography image processing system as defined in claim 19 wherein said processor firstly registers a functional component of said atlas with said emission tomography images to generate a set of spatial transformation parameters and then registers the anatomical component of said atlas with said emission tomography images using said set of spatial transformation parameters.

21.		An emission tomography image processing system as defined in claim 20 wherein said functional component simulates a SPECT or PET scan of said region of interest

and wherein said anatomical component simulates a transmission scan of said region of interest.

22.   An emission tomography image processing system as defined in claim 21 wherein said memory stores a database of atlases.

23.   An emission tomography image processing system as defined in claim 22 wherein said processor selects an atlas from said database automatically based on the degree of registration of each atlas in said database with said emission tomography images.

24.   An emission tomography image processing system as defined in claim 23 wherein said processor performs a preliminary reconstruction of each atlas and registers the atlas to the preliminary reconstruction to determine the degree of registration of each atlas.

25.   An emission tomography image processing system as defined in claim 23 wherein said processor combines multiple atlases to yield a resultant atlas that better registers with said emission tomography images.

26.   An emission tomography image processing system as defined in claim 22 wherein said database includes disease specific atlases, physical trait specific atlases and/or tracer or lesion specific atlases.

27.   An emission tomography imaging system comprising:
    means for taking emission tomography images of a region of interest of a subject to form a three-dimensional image of said region of interest;
    memory to store said emission tomography images, said memory also storing at least one three-dimensional computer model of said region of interest, said computer model representing the density distribution within said region of interest; and
    a processor for aligning said computer model with said emission tomography images and for applying scatter and attenuation correction to said emission tomography images using said aligned computer model as a guide.

28.   A computer readable medium including computer program code for applying scatter and attenuation correction to emission tomography images of a region of interest of a subject, said computer readable medium including:

computer program code for aligning a three-dimensional computer model representing the density distribution within said region of interest with said emission tomography images; and

computer program code for applying scatter and attenuation corrections to said emission tomography images using said aligned computer model as a guide.

29.   A computer readable medium as defined in claim 28 wherein said computer program code for aligning includes:

computer program code for aligning a functional component of said computer model simulating a SPECT or PET scan of said region of interest and for generating a set of spatial transformation parameters; and

computer program code for aligning an anatomical component of said computer model simulating a transmission scan of said region of interest using said set of spatial transformation parameters.

Figure 1
Patient data

A

SPECT scan without scatter
and attenuation correction

B
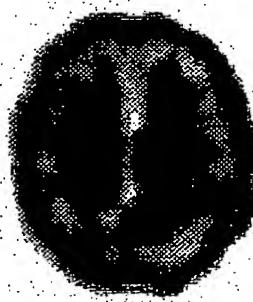
SPECT scan axial slice

C
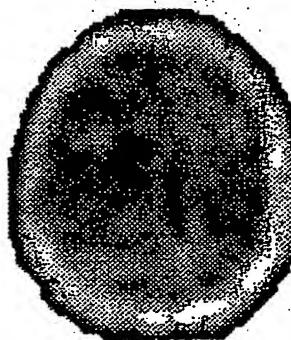
Transmission scan axial slice

D

Appurtenant anatomy for scatter
and attenuation correction (sagittal)

E
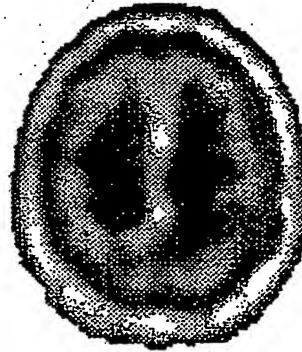
Appurtenant anatomy for scatter
and attenuation correction (transverse)

SUBSTITUTE SHEET (RULE 26)

Figure 2

50 Patient ────────────────────────▶ Emission reconstruction 52

                                                    │
                                                    ▼

                                          56
                          Calculate alignment of brain component
                          to emission reconstruction ◀──────┐
                                                             │
                                    │   │
                              Alignment   ┊   │
                              parameters   ┊   54 Head
                                    ┊   atlas
                                    ▼   │
60 Scatter and   ◀──   Apply alignment   ◀───────────┘
    attenuation   to entire atlas
    corrections
                                          58
        │
        ▼

62 Emission
    reconstruction

        │
        ▼

64 Patient scan
    analysis
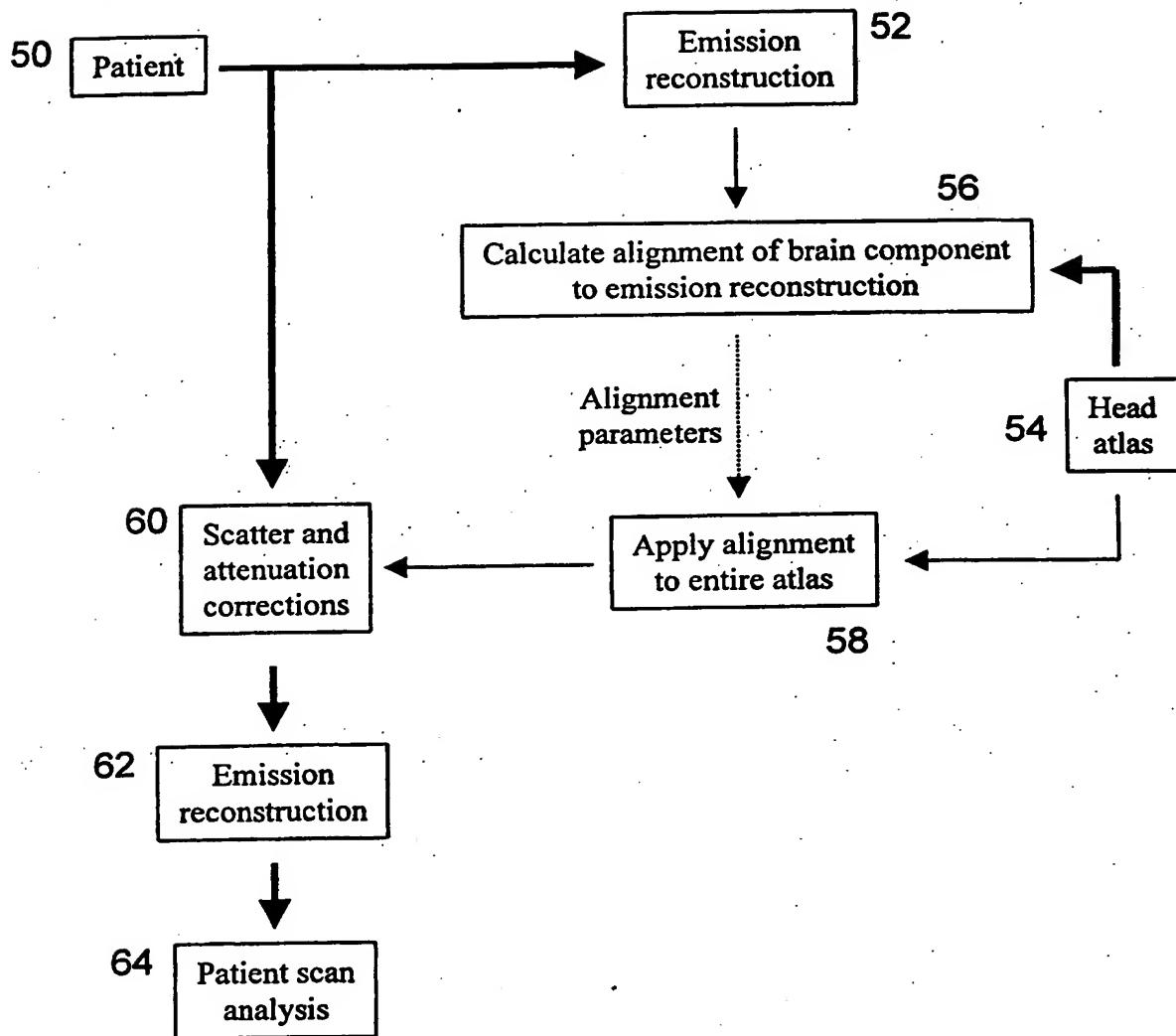
SUBSTITUTE SHEET (RULE 26)

Figure 3
Phantom data

A
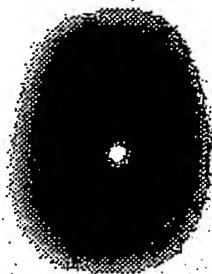
SPECT scan (transverse)

B
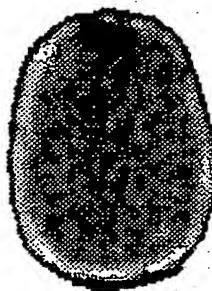
Transmission scan (transverse)

C

Appurtenant anatomy for
scatter and attenuation correction
(sagittal)

D
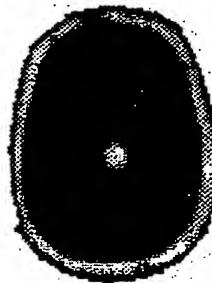
Appurtenant anatomy for
scatter and attenuation correction
(transverse)

E

Inferred anatomy for
scatter and attenuation correction
(sagittal)

F
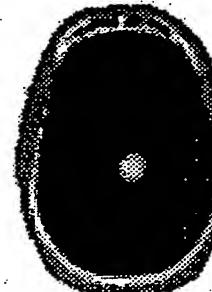
Inferred anatomy for
scatter and attenuation correction
(transverse)

SUBSTITUTE SHEET (RULE 26)

Figure 4

A
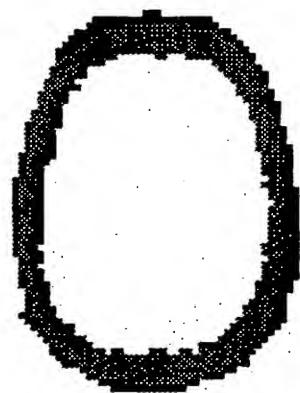
Slice 80

B
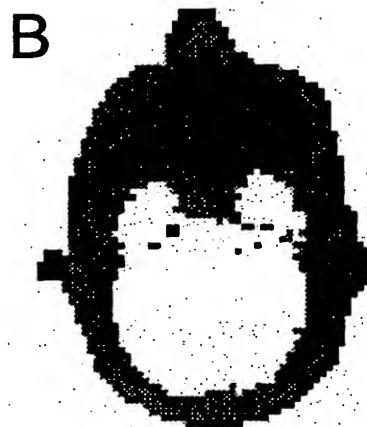
Slice 94

(A) Mid-cortical and (B) cerebellar transverse slices.
Volume enclosed by brain contour (white), appurtenant
anatomy (gray), and inferred anatomy (black).
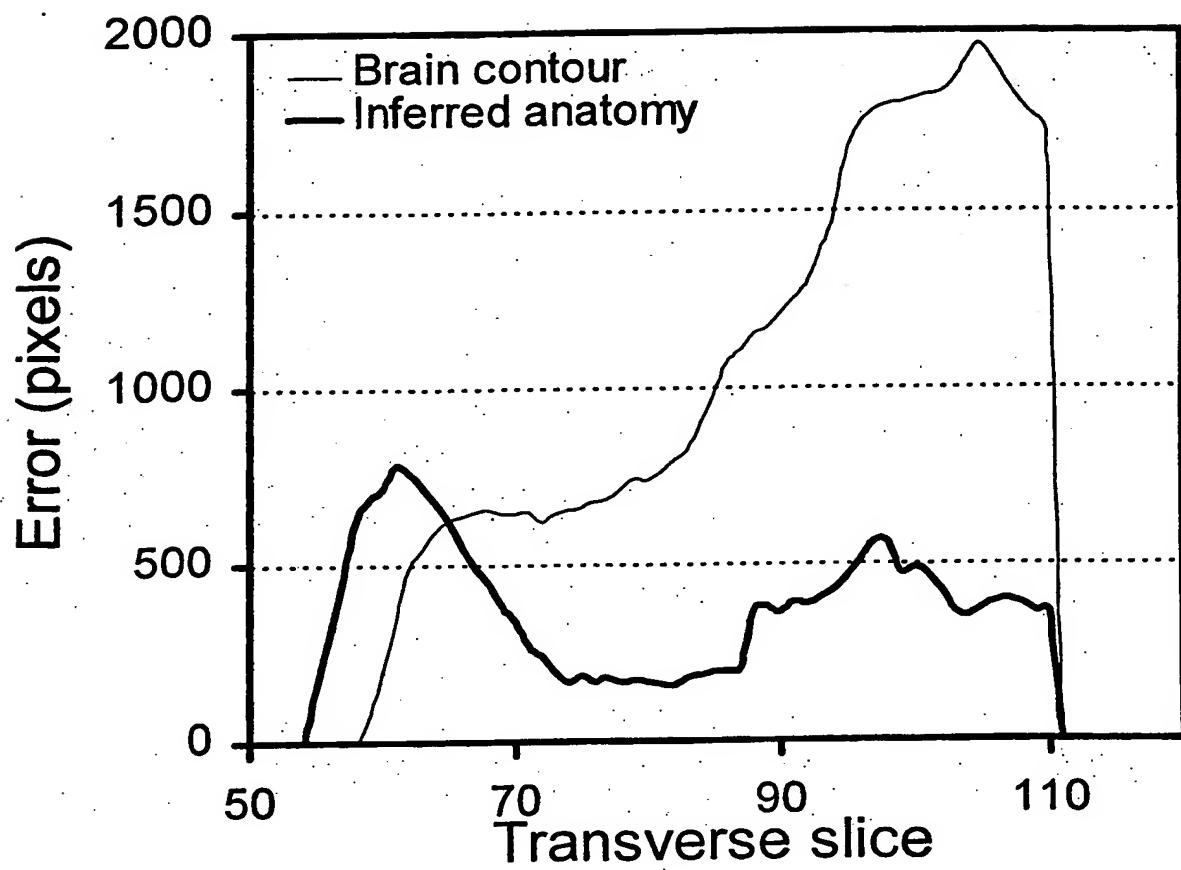
Both the brain contour and uniform inferred anatomy differ
from appurtenant anatomy. Here, this difference (in pixels)
is plotted as a function of transverse slice.

A

B
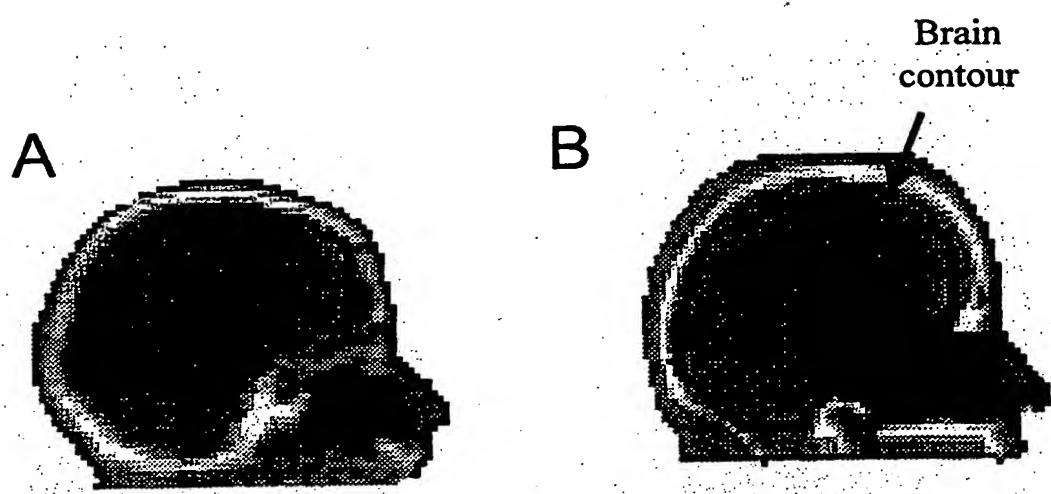
Brain
contour

Sagittal slice through (A) appurtenant anatomy and
(B) inferred anatomy. The (appurtenant) brain contour
is shown as the thick black outline in both (A) and (B).

Figure 7

A
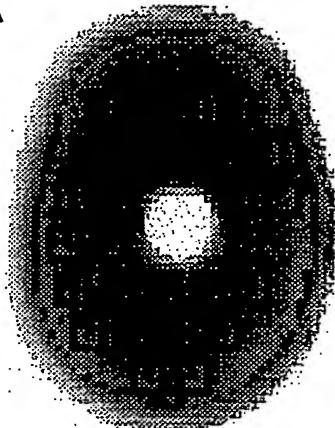
SPECT scan of the head phantom. (transverse slice)
Black squares in (A) are a subset of the two-hundred
macrovoxels defined in the reconstructed volume.
The macrovoxels are used in the error metrics
defined below.

B
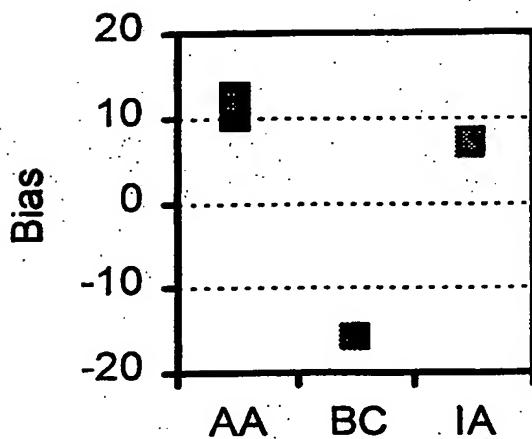
Global bias, shown in (B), was defined as
[(mean macrovoxel activity/calibration)-1]*100%.
Data is shown for appurtenant anatomy (AA),
braincontour (BC), and inferred anatomy (IA).
Uniform corrections are shown in gray, and
non-uniform in black.

C

Global uniformity, shown in (C), was defined as
[(coefficient of variation of macrovoxels)*100%].
Data is shown for appurtenant anatomy (AA),
braincontour (BC), and inferred anatomy (IA).
Uniform corrections are shown in gray, and
non-uniform in black.
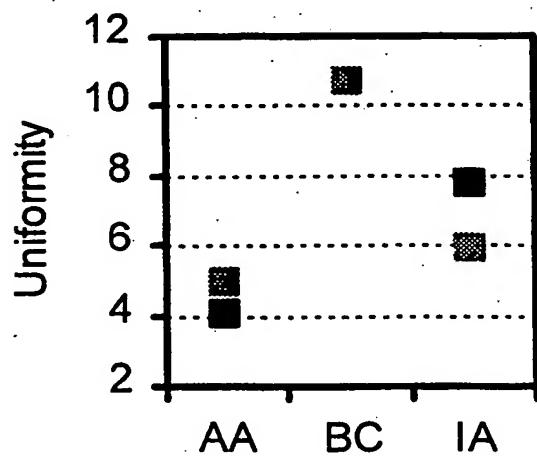
Figure 8

A
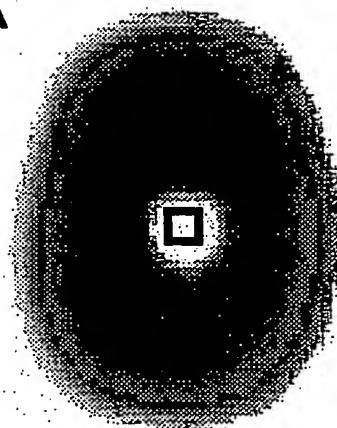
(A) SPECT scan of phantom (transverse slice at cortical level). Hot and cold regions of interest were defined (hot at centre). The regions were used to calculate contrast recovery and relative quantification, as described in (B) and (C) below.

B
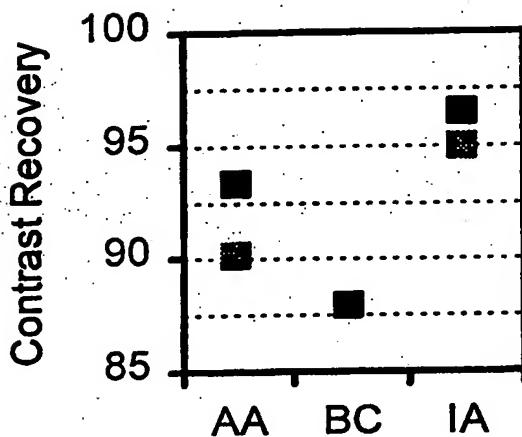
Contrast recovery (B) was calculated as [(Hot / Cold activity) / true activity ratio]*100%. Data is shown for appurtenant anatomy (AA), brain contour (BC), and inferred anatomy (IA).

Relative quantification (cortical:cerebellar activity ratio - regions of interest not shown) is presented in (C). Data is shown for appurtenant anatomy (AA), brain contour (BC),and inferred anatomy (IA).

C
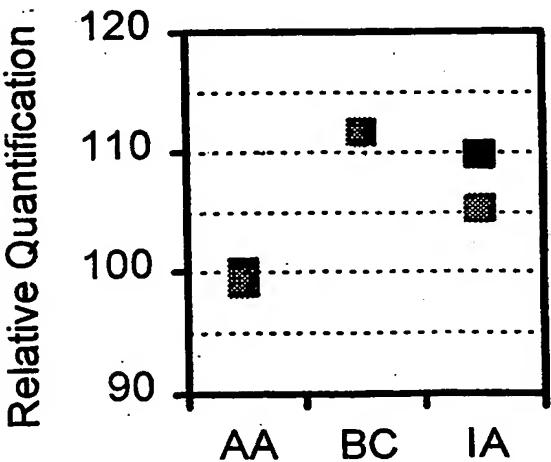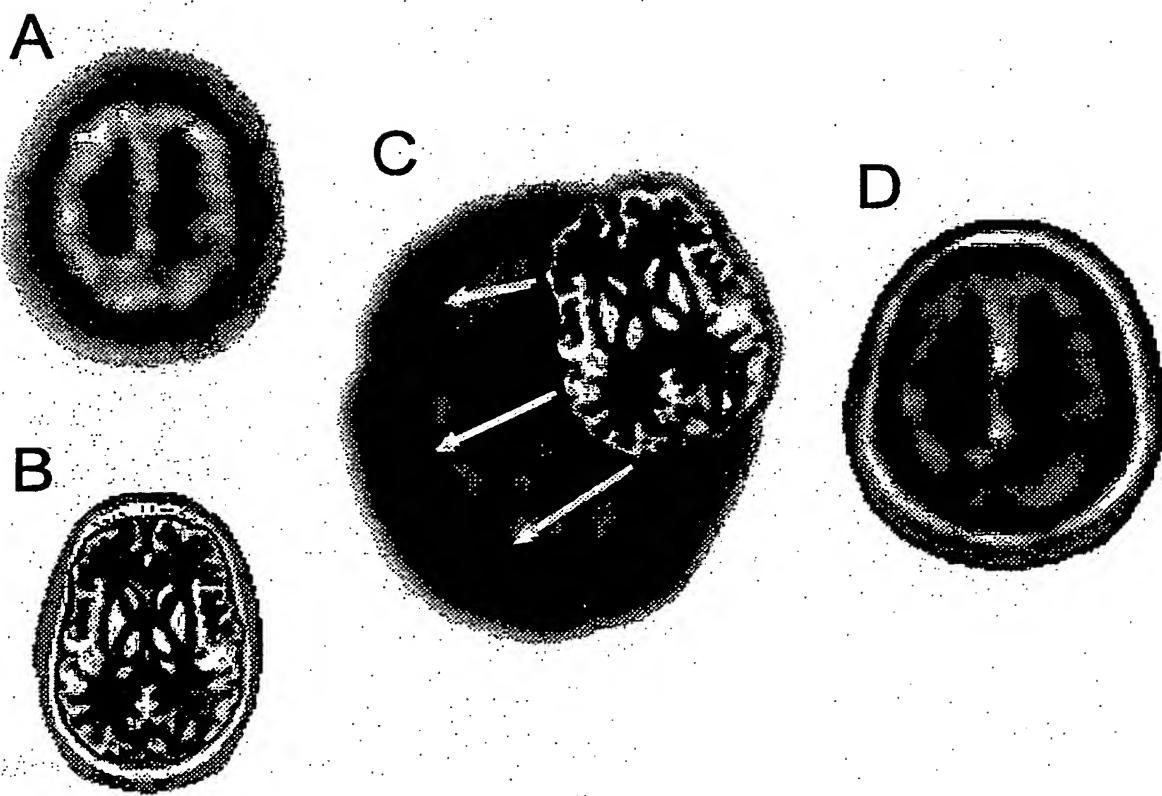
The Inferred Anatomy algorithm requires a patient's preliminary reconstruction (**A**) and a head atlas (**B**). The preliminary reconstruction does not include scatter and attenuation correction. The head atlas consists of a functional component (brain), and an anatomical component (extra-cerebral tissue). The functional component is then spatially registered to the preliminary reconstruction (**C**), and this optimal transformation is recorded. The patient's anatomy is then inferred by applying the same transformation to the anatomical component of the head atlas (**D**).

Figure 10

A
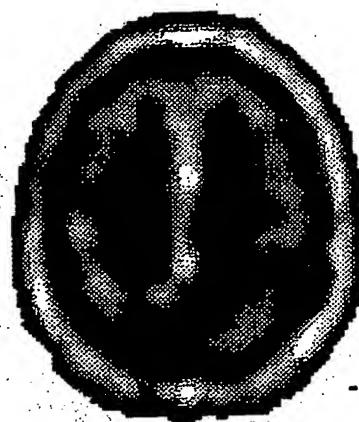
B
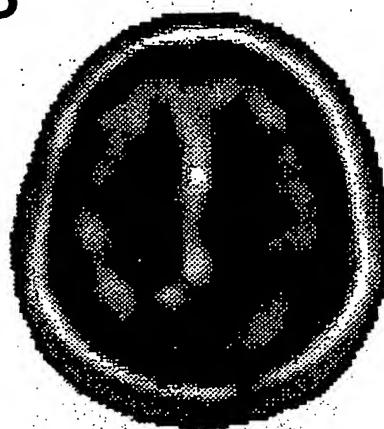
C

D

Examples of a patient's SPECT scan (brain) superimposed onto the pertinent transmission reconstruction (**A** and **C**, extra-cerebral tissue) and Inferred Anatomy (**B** and **D**, extra-cerebral tissue). The reconstruction includes scatter and attenuation correction guided by either the transmission reconstruction or Inferred Anatomy.

Figure 11
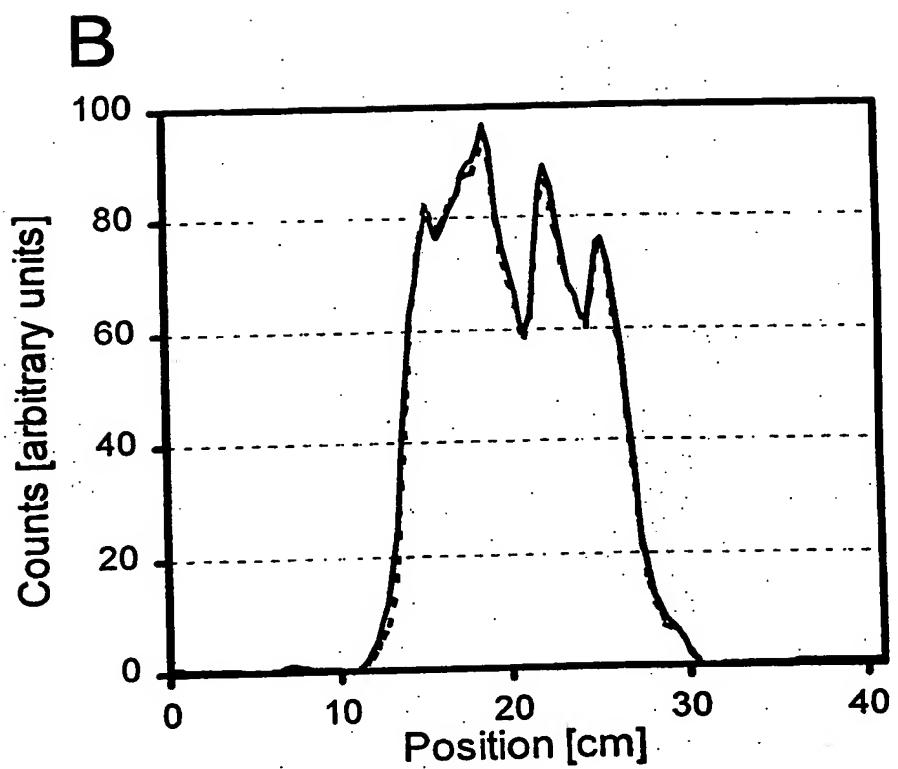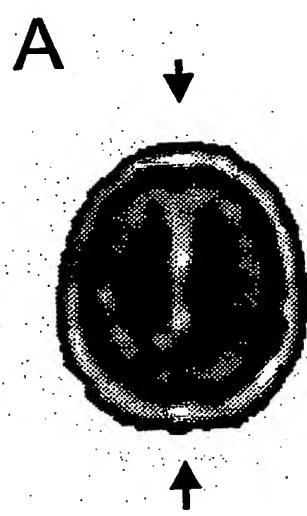
Profiles (**B**) through reconstructions at the cortical-axial level (**A**) comparing a SPECT reconstruction guided by the pertinent transmission scan (solid) with the reconstruction guided by Inferred Anatomy (dots). The profiles were taken between the two arrows in **A**.

Figure 12
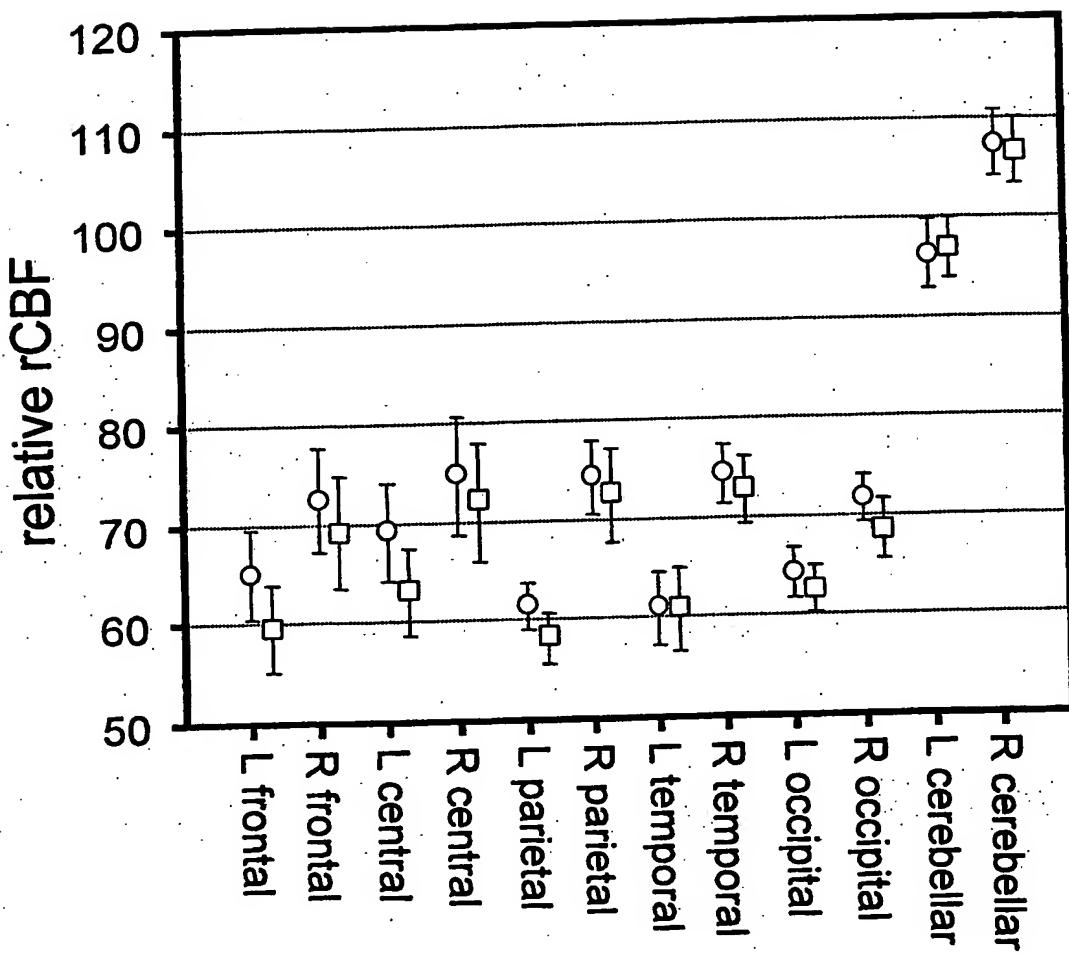
Regional ceebral blood flow with voxel-by-voxel Lassen's correction, relative to the cerebellum is shown for the twelve bilateral regions-of-interest. Means and standard errors are calculated across the ten patients. The quantification follows scatter and attenuation correction guided by transmission reconstructions (circles) or Inferred Anatomy (squares).

Figure 13
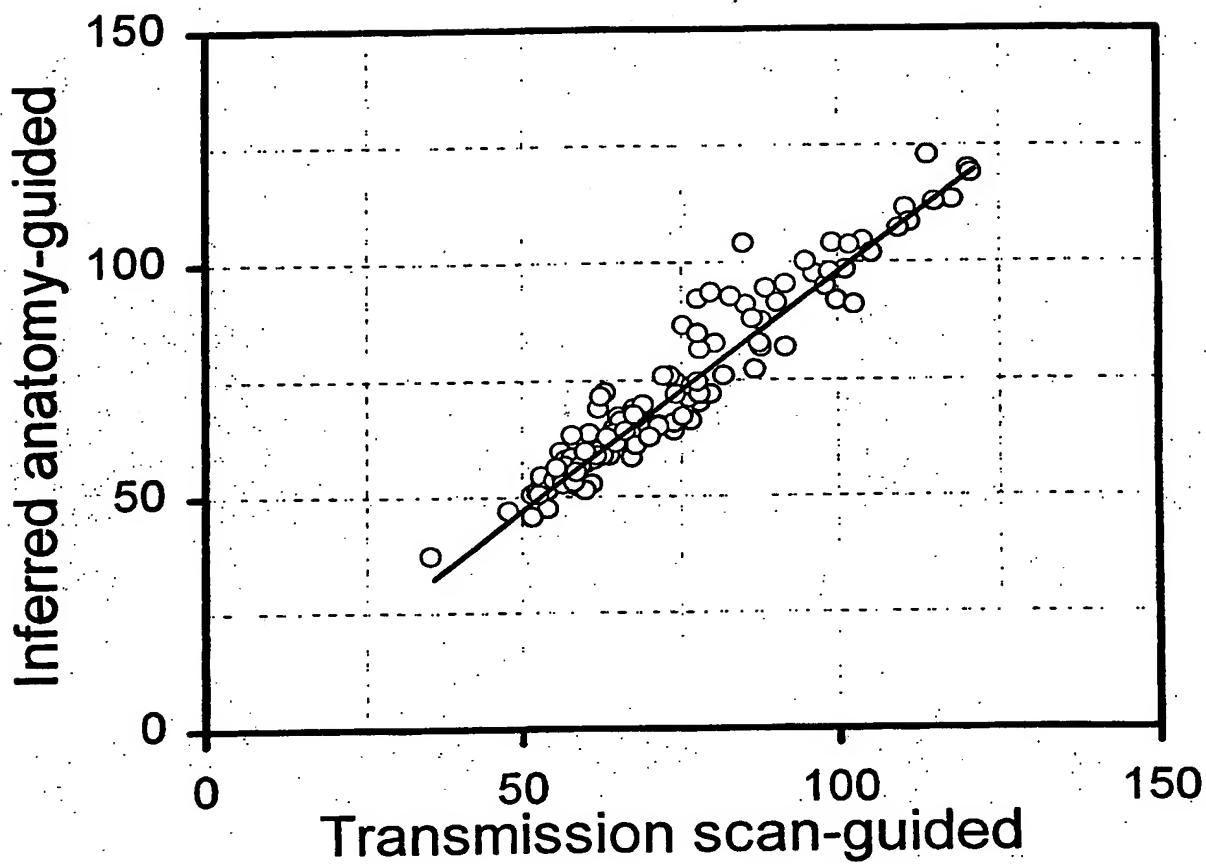
Comparison of reconstructions guided by transmission scans (abscissa), with reconstructions guided by Inferred Anatomy (ordinate). 120 data points are shown; these are from twelve regions-of-interest and ten patients. Each point represents regional cerebral blood flow with Lassen's correction, relative to the cerebellum. The equation of the line-of-best-fit is y=1.02x-3.83, and the correlation coefficient squared is $r^2=0.92$ (p<<0.0001).

INTERNATIONAL SEARCH REPORT

A. CLASSIFICATION OF SUBJECT MATTER
IPC 7   G01T1/164

According to International Patent Classification (IPC) or to both national classification and IPC

B. FIELDS SEARCHED

Minimum documentation searched (classification system followed by classification symbols)

IPC 7   G01T

Documentation searched other than minimum documentation to the extent that such documents are included in the fields searched

Electronic data base consulted during the international search (name of data base and, where practical, search terms used)

C. DOCUMENTS CONSIDERED TO BE RELEVANT

Category °	Citation of document, with indication, where appropriate, of the relevant passages	Relevant to claim No.
A	S.L. BACHARACH, ET AL: "Attenuation correction in cardi" JOURNAL OF NUCLEAR CARDIOLOGY, vol. 2, no. 3, June 1995 (1995-06), pages 246-255, XP002125238 St Louis, USA cited in the application page 247, column 2, line 5 -page 248, column 1, line 6; figure 2	1

☐ Further documents are listed in the continuation of box C.   ☐ Patent family members are listed in annex.

* Special categories of cited documents :

"A" document defining the general state of the art which is not considered to be of particular relevance

"E" earlier document but published on or after the international filing date

"L" document which may throw doubts on priority claim(s) or which is cited to establish the publication date of another citation or other special reason (as specified)

"O" document referring to an oral disclosure, use, exhibition or other means

"P" document published prior to the international filing date but later than the priority date claimed

"T" later document published after the international filing date or priority date and not in conflict with the application but cited to understand the principle or theory underlying the invention

"X" document of particular relevance; the claimed invention cannot be considered novel or cannot be considered to involve an inventive step when the document is taken alone

"Y" document of particular relevance; the claimed invention cannot be considered to involve an inventive step when the document is combined with one or more other such documents, such combination being obvious to a person skilled in the art

"&" document member of the same patent family

Date of the actual completion of the international search	Date of mailing of the international search report
28 December 1999	13/01/2000

Name and mailing address of the ISA	Authorized officer
European Patent Office, P.B. 5818 Patentlaan 2 NL – 2280 HV Rijswijk Tel. (+31-70) 340-2040, Tx. 31 651 epo nl, Fax: (+31-70) 340-3016	Anderson, A

Form PCT/ISA/210 (second sheet) (July 1992)

1